




# Overview of the Chang'e-4 Mission: Opening the Frontier of Scientific Exploration of the Lunar Far Side

Chunlai Li<sup>1,2</sup> · Wei Zuo<sup>1,2</sup>  · Weibin Wen<sup>1</sup> · Xingguo Zeng<sup>1</sup> · Xingye Gao<sup>1</sup> · Yuxuan Liu<sup>1</sup> · Qiang Fu<sup>1</sup> · Zhubin Zhang<sup>1</sup> · Yan Su<sup>1,2</sup> · Xin Ren<sup>1</sup> · Fang Wang<sup>1</sup> · Jianjun Liu<sup>1,2</sup> · Wei Yan<sup>1</sup> · Xu Tan<sup>1</sup> · Dawei Liu<sup>1</sup> · Bin Liu<sup>1</sup> · Hongbo Zhang<sup>1</sup> · Ziyuan Ouyang<sup>1,3</sup>

Received: 27 March 2020 / Accepted: 9 January 2021 / Published online: 8 March 2021  
© The Author(s), under exclusive licence to Springer Nature B.V. part of Springer Nature 2021

**Abstract** China's Chang'e-4 (CE-4) mission is the first human lander/rover mission on the far side of the Moon. Its probe is composed of a lander, rover, and the Queqiao relay satellite. Queqiao was successfully launched on May 21, 2018, and entered the halo orbit of the L2 point on June 14, becoming the first satellite connecting the Earth and the Moon's far side. The lander carrying Yutu-2 was successfully launched on December 8, 2018, and landed in the Von Kármán crater (45.5° S, 177.6° E) at 10:26 (UTC+8) on January 3, 2019. The CE-4 probe carried nine science instruments. Four instruments are on the lander: a landing camera (LCAM), a terrain camera (TCAM), a low-frequency radio spectrometer (LFRS), and a lunar lander neutrons and dosimetry (LND) provided by Germany. Four instruments are on the rover: a panoramic camera (PCAM), a visible and near-infrared imaging spectrometer (VNIS), a lunar penetrating radar (LPR), and an advanced small analyzer for neutrals (ASAN) provided by Sweden. The instrument on the relay satellite is the Netherlands-China Low-Frequency Explorer (NCLE). The scientific objectives of the CE-4 mission include (1) performing low-frequency radio-astronomical observations; (2) investigating the geomorphology, mineral compositions and shallow subsurface structure of the landing and roving sites; and (3) detecting the Earth-Moon space environment at the lunar far side. As of February 1, 2020, CE-4 has completed 14 lunar days of scientific exploration after one year of operation. The components, flight, scientific objectives and investigation of CE-4 are introduced in this paper. We also describe the accessibility of the initial archived science data and their preliminary analysis results.

**Keywords** Moon · Chang'e-4 · Spacecraft · Mission design

---

✉ W. Zuo  
zuowei@nao.cas.cn

<sup>1</sup> Key Laboratory of Lunar and Deep Space Exploration, National Astronomical Observatories, Chinese Academy of Sciences, Beijing 100101, China

<sup>2</sup> University of Chinese Academy of Sciences, Beijing 100049, China

<sup>3</sup> Institute of Geochemistry, Chinese Academy of Sciences, Guiyang 550081, China

## 1 Introduction

China's Chang'e-4 (CE-4) probe successfully landed on the floor of the Von Kármán crater (45.5° S, 177.6° E) at 10:26 (UTC+8) on January 3, 2019 (Wu et al. 2019). It is the first spacecraft that has ever soft-landed on the far side of the Moon. The first image of the lunar far side was obtained by the Soviet spacecraft Luna 3 on October 4, 1959. Since then, humans have explored the lunar far side more than 30 times by means of encircling and overflight. Twenty soft-landing missions were carried out to explore the Moon. However, they were all targeted at the surface of the lunar near side (Wu et al. 2019), and none of them had ever landed on the surface of the lunar far side. The CE-4 mission includes a lander and a rover as well as a relay satellite located at the L2 point of the Earth-Moon system. Relay communication was realized over a distance of 500,000 km between the lunar far side and the Earth, opening a new horizon for human lunar exploration.

The CE-4 lander and its rover, Yutu-2, are the first visitors of the lunar far side from the Earth. The designed mission times for Yutu-2 and the lander are three months and one year, respectively. In contrast, the relay satellite, Queqiao, will continue operating for three years (Wu et al. 2017). To fulfill the scientific objectives of the CE-4 mission, the China National Space Administration (CNSA) solicited proposals for instruments on board CE-4 and coordinated the processes regarding payload evaluation, construction, and management. Nine scientific instruments were selected for the CE-4 mission. The lander includes a landing camera (LCAM), a terrain camera (TCAM), a low-frequency radio spectrometer (LFRS), and a lunar lander neutron and dosimetry (LND) instrument from Germany. Yutu-2 has a panoramic camera (PCAM), a visible and near-infrared imaging spectrometer (VNIS), a lunar penetrating radar (LPR), and an advanced small analyzer for neutrals (ASAN) from Sweden. The Netherlands-China Low-Frequency Explorer (NCLE), developed by the Netherlands, is installed on the Queqiao relay satellite (Ye et al. 2017). As of February 1, 2020, the lander and the rover have completed the scientific exploration of 14 lunar days after one year of operation. Currently, the lander and the rover are working normally and will perform follow-up scientific exploration tasks.

In this review, we introduce the flight and landing processes of the CE-4 mission (Sect. 2), present its objectives and instrument capabilities (Sect. 3), summarize the mission implementation (Sect. 4) and explain the scientific data management procedures (Sect. 5). Finally, a summary of preliminary results is provided (Sect. 6).

## 2 Mission Description

CE-4 was originally planned as a backup for the Chang'e-3 (CE-3) mission. In 2014, the CNSA carried out an investigation on the adjustment of the CE-4 mission after the success of the CE-3 mission. In January 2016, the CE-4 mission was officially implemented. The relay satellite was designed to be located at the L2 point of the Earth-Moon system (Fig. 1). The landing site of the lander and rover was planned as the floor of the Von Kármán crater within the South Pole-Aitken (SPA) basin on the lunar far side to carry out in situ detection and reconnaissance.

### 2.1 Components of the CE-4 Probe

As mentioned above, the CE-4 probe is composed of a lander, a rover, and a relay satellite, as shown in Fig. 2. The rover is called Yutu-2, and the relay satellite is called Queqiao.

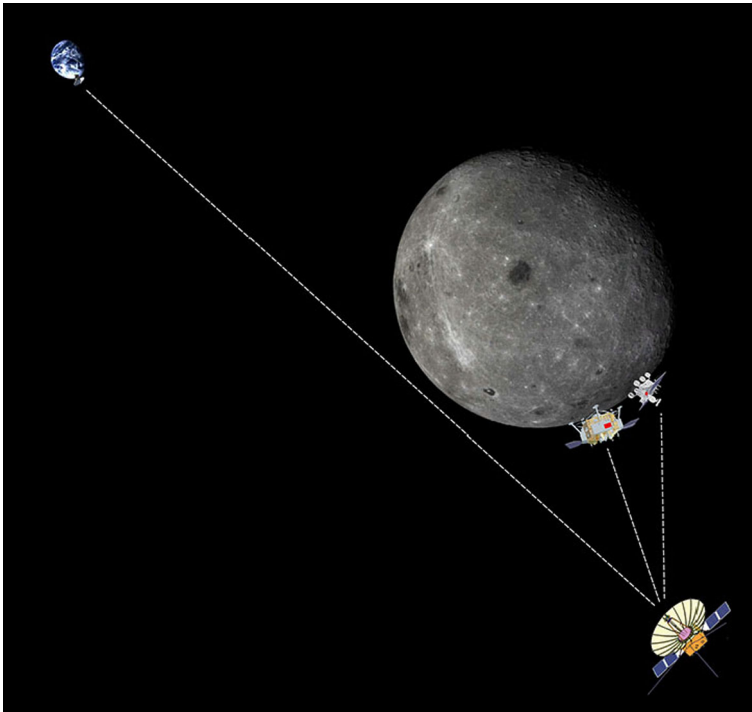


**Fig. 1** The CE-4, exploring the far side of the Moon, with its lander, rover, and relay satellite

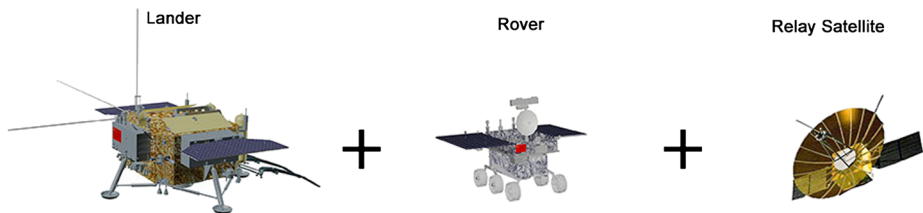


**Fig. 2** The schematic diagram of the CE-4 probe components

The CE-4 probe is designed and optimized with the addition of important hardware and software modifications, including an improvement to the navigation and control technique for lunar far-side landing, an update to the telemetry, tracking and control (TT&C) system for relay communication, and an adjustment to the payload configuration for international cooperation. Moreover, a radioisotope thermoelectric generator (RTG) is added, while the radioisotope heater unit (RHU) is preserved. The RTG together with the RHU can supply no less than 2.5 W of electric power (Ye et al. 2019).

The lander is composed of measuring equipment for engineering parameters and 11 sub-systems: the structure and mechanism; landing buffering; thermal control; primary power supply; overall circuit; TT&C/data transmission; guidance, navigation and control (GNC); propulsion; data management; directional antenna; and payload subsystems. The weight of the lander is 1200 kg, and the designed lifetime is six months. The eight subsystems of the rover are the locomotion, structure and mechanism, GNC, integrated electronic, power sup-

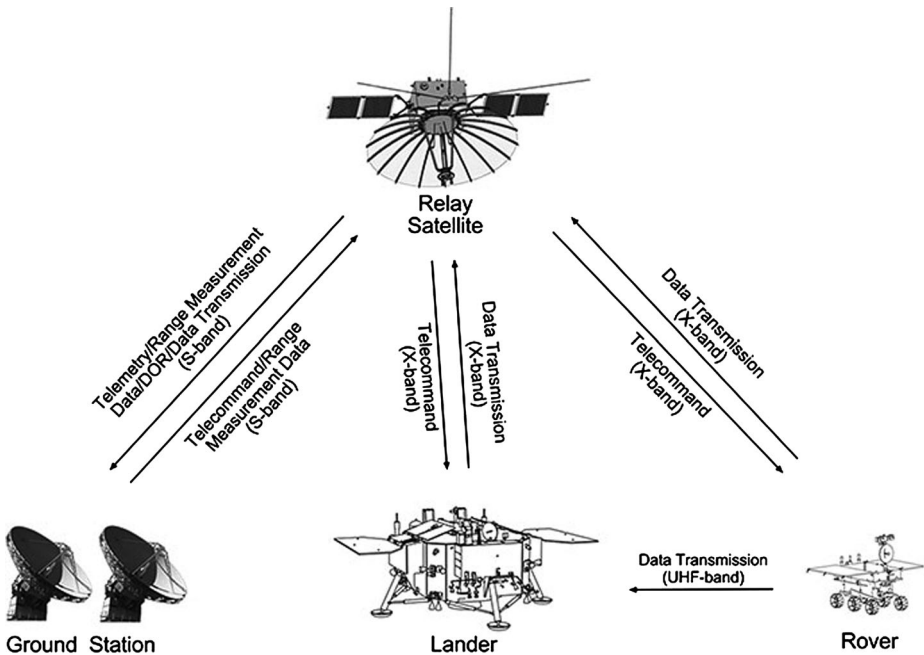


**Fig. 3** The schematic diagram of the communication links between the relay satellite, lander, rover, and the ground stations

ply, thermal control, TT&C/data transmission, and payload subsystems. The weight of the rover is 140 kg, and the designed lifetime is three months. The lander and the rover were launched as a combination, and the total mass of the lander/rover combination is 3780 kg (Ye et al. 2019).

Queqiao plays a key role in lunar far-side exploration. It is rectangular in shape, and a plate structure was adopted with a 4.2-m umbrella antenna on the top. To obtain a three-axis stabilized satellite control, a star sensor and a fiber-optic gyroscope are used in the zero-momentum attitude control system. Queqiao exhibits quasiperiodic motion at the Earth-Moon L2 point (the amplitude of the Z-axis is approximately 13,000 km). The X band is adopted for communication between the lander/rover and Queqiao. An ultra-high-frequency (UHF) radio link is adopted for communication between the lander and the rover. The S-band is utilized for data transmission from Queqiao to the ground. The details of the communication links can be seen in Fig. 3.

## 2.2 Flight of the CE-4 Probe

The CE-4 mission included two launches. The first launch was for Queqiao, which was planned for the first half of 2018. The second launch was for the lander and rover, which was scheduled for early 2019.

### 2.2.1 Flight of the Relay Satellite

Queqiao was launched by a Long March 4C rocket on May 21, 2018, from Xichang Satellite Launch Center. After one midway correction and braking at perilune, it arrived at the Earth-Moon L2 point. It entered the halo orbit of the L2 point on June 14 after the third acquisition

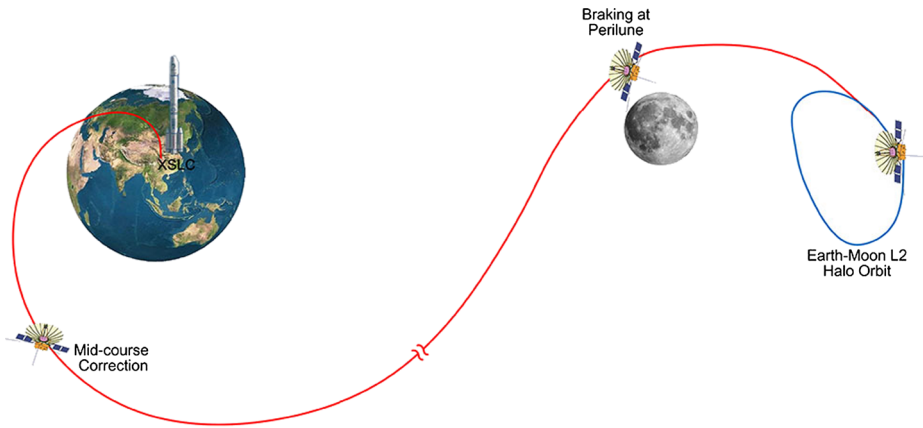


**Fig. 4** The schematic diagram of the Queqiao's flight process

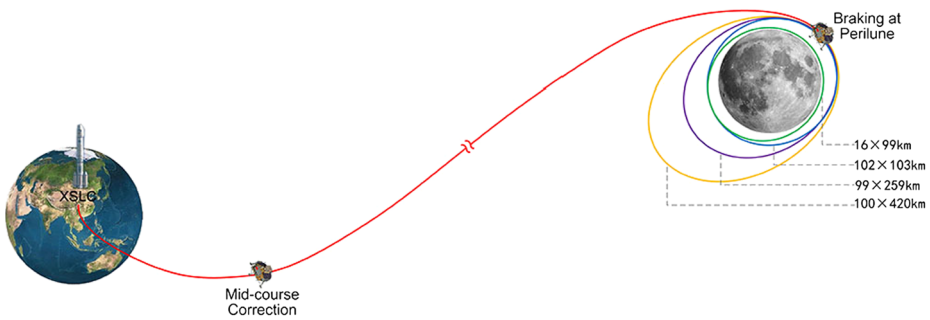


**Fig. 5** Illustration of the lunar orbit entry process of the CE-4 probe

control step (Fig. 4). By the end of July, all in-flight tests were completed, and Queqiao had the capacity to communicate with the detector on the far side of the Moon and with the ground station on Earth. It realized relay communication in outer space and became the first satellite that connects the Earth to the Moon's far side.

**2.2.2 Lunar Orbit Entry Process of the CE-4 Probe**

The CE-4 probe was launched by a Long March 3B rocket on December 8, 2018, at 23:23:34 (UTC+8) from Xichang Satellite Launch Center. It entered the Earth-Moon transfer orbit as scheduled with a perigee of 200 km and an apogee of 420,000 km. On December 9, it completed orbital correction. On December 12, it completed braking at perilune by a 7500N engine and entered the 100x420-km lunar orbit with an inclination of 85.4°. After three adjustments, it entered the 16x99-m lunar orbit on December 30, 2018 (Fig. 5).

**2.2.3 Landing Process of the CE-4 Probe**

Achieving the soft-landing at an altitude of 15 km was the most dangerous and complicated process of the CE-4 mission. Because of an apparent larger variation in the elevation of flight tracks compared to that of CE-3 (increased from 3 km to 7 km), landing control becomes

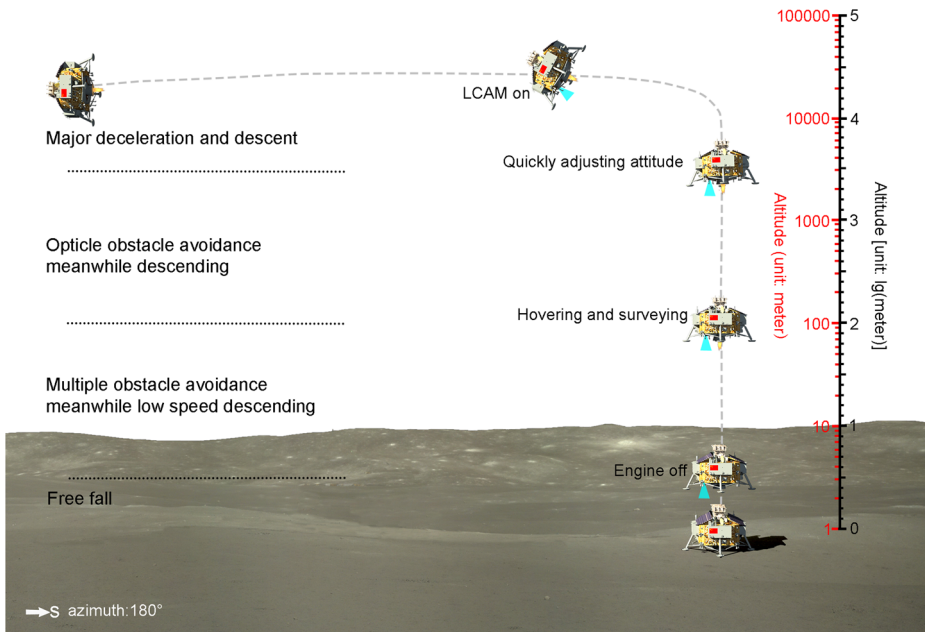


**Fig. 6** The soft-landing process of the CE-4 lander/rover combination

extremely difficult. Therefore, a new design (Sun et al. 2019) was adopted in the landing process and is shown in Fig. 6.

The CE-4 probe began its soft landing on January 3, 2019. The communication link between the probe and relay satellite became active at 9:34, and the probe entered the far-side orbit at 9:41. The 7500N engine started working at 10:14, entering the primary deceleration phase and starting the powered descent. Then, it sequentially performed the approaching descent at 10:23, hovering at 10:25, and obstacle avoidance at 10:25. Finally, the CE-4 probe successfully landed on the surface of the Moon at 10:26:02. The whole powered descent process lasted 687 s.

### 3 CE-4 Mission Science Objectives

CE-4 has nine scientific payloads (Table 1): five payloads (TCAM, LCAM, PCAM, LPR, and VNIS) inherited from CE-3 and four new payloads. Three of the new payloads are international scientific payloads: the LND instrument from Germany, the ASAN from Sweden, and the NCLE from the Netherlands. The objectives of the CE-4 mission are (1) to perform low-frequency radio-astronomical observations; (2) investigate the geomorphology, mineral compositions, and shallow structure of the landing and roving sites; and (3) to detect the lunar environment, such as neutral atoms and their dose, at the far side of the Moon (Table 2).

#### 3.1 Low-Frequency Radio-astronomical Study of the Lunar Surface

The Moon, in contrast to Earth, has an extremely thin ionosphere allowing radio-frequency measurements of its surface at 500 kHz during the day and even lower during the night

**Table 1** Technical and performance parameters of the CE-4 payloads

Platform	Instrument	Major technical characteristics	Major performance characteristics
Lander	Terrain Camera (TCAM)	Spectral range: 420–700 nm Imaging modes: color static, color video Effective pixel number: 2,352 × 1,728 FOV: 22.9° × 16.9°	Imaging distance: 5 m–∞ Quantization: 8 bit Video frame rate: 5–10 fps
	Landing Camera (LCAM)	Spectral range: 419–777 nm Effective pixel number: 1,024 × 1,024 FOV: 45° × 45°	Imaging distance: 4 m–∞ Quantization: 8 bit Frame rate: 10 fps
	Low-Frequency Radio Spectrometer (LFRS)	Frequency: 0.1 ~ 40 MHz Receiver sensitivity: ≤ 10 nV/√Hz Dynamic Range: ≥ 75 dB	Frequency resolution ≤ 10 KHz (frequency 0.1 ~ 2.0 MHz) ≤ 200 KHz (frequency 1.0 ~ 40 MHz)
	Lunar Lander Neutrons & Dosimetry (LND)	Fast neutron spectra: 1-20 MeV Thermal neutrons flux: 10-104/min Proton spectra: 7-30 MeV Charged particle spectra: 60-500 KeV α spectra: 7-20 MeV Heavy particle spectra: 10-30 MeV/n LET-spectral range: 0.1-430 KeV/μm	Temporal resolution: Dose rate 1 min, Proton 5 min, Charged particle 5 min, Heavy particle 30 min
Rover	The Panoramic Camera (PCAM)	Spectral range: 420–700 nm Imaging modes: color and panchromatic Effective pixel 0 number: 2,352 × 1,728 (color mode), 1,176 × 864 (panchromatic mode) FOV: 19.7° × 14.5°	Imaging distance: 3m–∞
	Lunar Penetrating Radar (LPR)	Center frequency: 60 MHz (1st channel), 500 MHz (2nd channel) Band width: ≥ 40 MHz (1st channel), ≥ 450 MHz (2nd channel)	Depth range: ≥ 100 m (1st channel), ≥ 30 m (2nd channel) Vertical resolution: ~ 1 m (1st channel), ≤ 30 cm (2nd channel)
	VIS-NIR Imaging Spectrometer (VNIS)	Spectral range: 450–950 nm(Vis-NIR), 900–2,400 nm (IR) Spectral resolution: 2–10 nm(Vis-NIR), 3–12 nm (IR)	Detection distance: 0.7–1.3 m Quantization: 10 bit
	Advanced Small Analyzer for Neutrals (ASAN)	Energy range: 10eV-10KeV	Mass resolution: Cation: mass-to-charge ratio of the ions equal to 1,2,4,8,16,32 Energy neutral atom: H, heavy atom Energy resolution: Energy neutral atom: 30%±10% Cation: 7%±2% temporal resolution: 10 s
Relay satellite	Netherlands-China Low frequency Explorer (NCLE)	Frequency band: 0.08-80 MHz Receiver sensitivity: < -160 dBm/Hz @ 10 MHz	Frequency resolution: 1 KHz@0.1-2.0 MHz 10 KHz@1-10 MHz 100KHz@10-80 MHz

**Table 2** The CE-4 science objectives and corresponding instruments capabilities

Science objective	Science exploration tasks	Contributing instruments		
		Lander instruments	Rover instruments	Relay satellite instrument
Low-frequency radio astronomical observation	Detect the solar low frequency radio radiation (0.1~40 MHz) Detect the low frequency radio radiation from other celestial body in solar system and galaxy (0.1~80 MHz)	Low-Frequency Radio Spectrometer (LFRS)		Netherlands-China Low frequency Explorer (NCLE)
Geomorphology, mineral compositions, shallow subsurface structure of and near the landing area	3D imagery In-situ analysis of chemical composition (element content and distribution) In-situ analysis of mineral compositions (mineralogical content and distribution) Regolith thickness and shallow subsurface structure	Landing Camera (LCAM) Terrain Camera (TCAM)	The Panoramic Camera (PCAM) VIS-NIR Imaging Spectrometer (VNIS) Lunar Penetrating Radar (LPR)	
Experimentally detect the lunar environment at far side of the lunar, such as dosage neutron, neutral atom	Measure the electrically neutral component, neutrons and $\gamma$ -rays. Measure the fast neutron flux and thermal neutrons flux In-situ analysis of energy neutral atom and cation	Lunar Lander Neutrons & Dosimetry (LND)	Advance Small Analyzer for Neutrals (ASAN)	

(Bums et al. 1989; Basart and Burns 1990). No radio signal from the earth's surface can reach the far side of the Moon due to its obstruction, meaning that the radio environment on the lunar far side is immaculate and may have radio signals only from nonhuman sources. For these reasons, the far side of the Moon has been widely considered an excellent site for low-frequency radio astronomy since the 1960 s (Bely et al. 1997; Takahashi 2003; Jester and Falcke 2009; Bandyopadhyay et al. 2018).

The low-frequency radio-astronomical observations will be jointly conducted by the LFRS and NCLE, taking advantage of the unique radio environment of the lunar far side (Arts et al. 2019). The LFRS explores the radio emissions from the Sun and lunar surface at very low frequencies (100 kHz~40 MHz). The NCLE investigates the use of low-frequency acquisition and ranging (LOFAR) to support the LFRS. As an unexplored portion of the electromagnetic spectrum, low-frequency radio measurements of the far side of the Moon will elucidate several processes, including magnetic structures of exoplanets and the red-shifted neutral hydrogen (HI) 21-cm line at redshifts  $z \geq 35$ , and thus to the so-called "dark ages" (Burns et al. 2012; Boonstra et al. 2016) that preceded the epoch of reionization in our universe.

### 3.2 Morphological, Compositional, and Geological Structure Investigation

Five instruments, namely, the LCAM, TCAM, PCAM (on the lander), VNIS, and LPR (on the rover), work cooperatively to investigate the geomorphology, mineral compositions, and shallow subsurface structure of the landing area, providing new evidence on the composi-



tion of the lunar mantle and advancing our understanding of the evolutionary history of the Moon.

### 3.2.1 *Geomorphology Investigation*

There is an obvious difference between the geological features of the near and far sides of the Moon (Wood 1973; Stevenson 1980; Miljković et al. 2013), the genesis of which remains uncertain. The LCAM can obtain images covering a few meters to over one hundred kilometers surrounding the landing area with the spatial resolution of the central pixel varying from a few millimeters to tens of meters during the descent process of the lander. It is capable of providing both large-scale and detailed background geomorphology information around the lander. The TCAM can take 360° panoramic images of the landing area and provide images for morphologic and topographic analyses. The PCAM can obtain continuous stereo images at a resolution on the decimeter scale along the reconnaissance path of the rover. The data obtained by the LCAM, TCAM, and PCAM are used to explore the landing area's topographic characteristics, such as the shape, distribution, and structure of surface craters and rocks, to reveal the possible lunar geological processes and lay the foundation for the subsequent detection tasks.

### 3.2.2 *Mineral Compositions Investigation*

The composition of the lunar crust and mantle and how they constrain the formation and evolutionary history of the Moon have remained unknown for many years (Ringwood 1979; Warren 1985; Pahlevan and Stevenson 2007; Khan et al. 2014). The landing area in the Von Kármán crater (diameter  $\approx 186$  km) is located within the SPA basin. The SPA basin, with a 2500-km diameter and a depth of 12 km, is the oldest, largest, and deepest impact crater on the Moon's surface (Wilhelms et al. 1987; Head et al. 1993). It is likely that the lower crust or upper mantle materials have been exhumed to the surface of the Moon, which is of essential significance for exploring the composition of deep-seated materials of the Moon. The VNIS of Yutu-2 enables the first in situ reflectance measurements of the far side of the Moon. It can acquire the reflectance spectra from 450 nm to 2400 nm with spectral resolutions ranging from 2.4 to 6.5 nm for hyperspectral imaging detectors (visible/near-infrared (VIS/NIR), 450~950 nm) and 3.6 to 9.6 nm for single-point spectrometers (shortwave infrared (SWIR), 900~2400 nm) (Li et al. 2019). Combining the topographical features captured by the LCAM, TCAM, and PCAM with the detected in situ mineralogy information acquired by the VNIS surrounding the reconnaissance path, the possible compositional difference between the landing site materials and the lunar near-side basalt can be compared. In addition, the composition of the lower crust and upper mantle can also be characterized by analyzing the materials ejected at the landing site during the impact events occurring after the formation of the SPA basin, which provides a theoretical basis for exploring the origin of the SPA basin and the early evolutionary history of the Moon (Huang et al. 2018).

### 3.2.3 *Shallow Subsurface Structure Investigation*

Knowledge of the stratigraphic architecture of the lunar subsurface is critical to understanding the shallow structure and composition of the lunar crust, the magnitude and history of volcanism, and surface modification processes. Previous investigations have shown that the thickness of the lunar soil within the Von Kármán crater is inhomogeneous due to varying degrees of lava material coverage originating from various stages of magma and material

ejection (Pieters et al. 1997; Petro and Pieters 2004; Vaughan and Head 2014). The LPR on Yutu-2 is a dual-frequency ground-penetrating radar (GPR) system operating at 60 and 500 MHz with corresponding bandwidths of 40–80 MHz and 250–750 MHz, respectively. It is designed to obtain information on the decimeter-scale structures of the regolith and the meter-scale structures of the upper crust along the excursion path (with a planned length of approximately 800 m), featuring several aspects of the CE-4 site. These aspects include the thickness and internal structure of the mare basalt fill, the nature of secondary crater ejecta layers in the landing area (where the material is deposited and re-excavated by distal ejecta from nearby craters), and the nature and structure of the regolith, such as the uppermost regolith layer and the buried regolith layers between flows.

### 3.3 Earth-Moon Space Environment Research

CE-4 will attempt to detect particle radiations of the lunar far side with the LND instrument and ASAN on board the lander and the rover, respectively. This mission is the first international cooperation between China and other nations in the areas of payload development, scientific exploration and research.

The major scientific goal of the LND experiment is to obtain the first active dosimetric measurements on the surface of the Moon. The LND instrument also provides observations of fast neutrons that are a result of the interaction of high-energy particle radiation with the lunar regolith and of their thermalized counterpart, thermal neutrons, which are a sensitive indicator of subsurface water content (Wimmer-Schweingruber et al. 2019, 2020). It measures the dynamic changes on the Moon's surface, providing the necessary support for the accurate assessment of radiation-related potential hazards (Reitz et al. 2012; Zhang et al. 2020a). In the meantime, it contributes to heliosphere research.

The ASAN is the first instrument to operate directly on the lunar surface and measure the energetic neutral atom flux originating from it. The ASAN measures with a single angular pixel the energy spectrum of energetic neutral atoms reflected or sputtered from the surface with coarse mass resolution (Wieser et al. 2020). It is used to explore the origin and distribution of the neutral atoms on the Moon's surface and the interaction mechanism between solar wind and the lunar surface, which is of fundamental importance in solving key problems such as the formation and maintenance mechanisms of the lunar escape layer (McComas et al. 2009; Zhang et al. 2020b).

## 4 Investigation of the CE-4 Mission

The CE-4 probe was launched by a Long March 3B rocket from the Xichang Satellite Launch Center in Sichuan Province on December 8, 2018. After aerobraking on December 12, the probe entered the lunar orbit, in which the perilune is 100 km and the apocynthion is 400 km away from the Moon. Through successful orbital controls, the CE-4 probe entered the scheduled preparation orbit on December 30 and stayed there for almost four days before it landed at Statio Tianhe (45.5° S, 177.6° E) ([https://planetarynames.wr.usgs.gov/Feature/15781?\\_fsk=-709402562](https://planetarynames.wr.usgs.gov/Feature/15781?_fsk=-709402562)) in the Von Kármán crater at 10:26 (UTC+8) on January 3, 2019. In total, 5441 images were taken by the LCAM to record the landing process. On the first lunar day, the Yutu-2 rover was separated from the lander at 15:07 on January 3. Then, it slowly moved to Point X. After that, when Yutu-2 arrived at Point A (left image in Fig. 7), the PCAM on the rover and the TCAM on the lander took a photo of each other for the first time. These two cameras took photos of each other

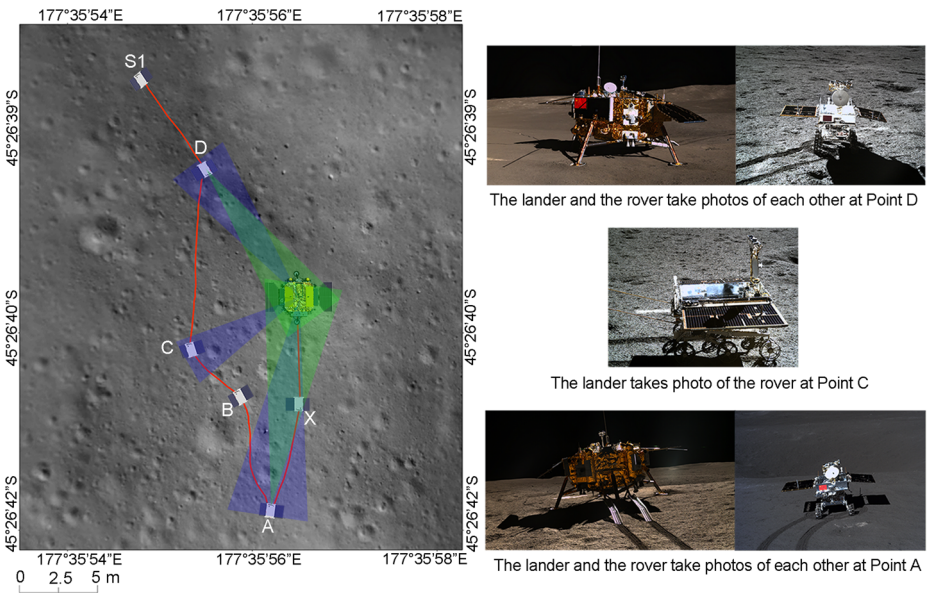


**Fig. 7** A map illustrating the lander and the rover taking photos of each other at Points A and D in the first lunar day. Left, the location of each point in the rover trace; right, the images acquired by them at a different point

for the second time when the rover arrived at point D after passing through Points B and C. All the instruments on the rover and the lander successfully obtained the data as planned on the first lunar day. On January 12, Yutu-2 was powered off at Point S1 before the cold lunar night, approximately 18 m northwest of the lander.

After the first lunar day, the follow-up exploration path of Yutu-2 was planned for the low-reflectance area to the west and northwest of the landing site. Specific lunar surface morphology and features such as fresh impact craters, basalt-covered areas, wheel tracks, rocks and potential ejecta were selected as the major detection targets, according to the exploration plan (Lin et al. 2019). As of February 1, 2020, Yutu-2 and the lander completed 14 lunar days of exploration and acquired much scientific data. The total travel distance of the rover was 367.3 m. Figure 8 shows Yutu-2's traverse path with a dormancy point labeled for illustration.

Each lunar day consists of several exploration points (white dots on the rover's path in Fig. 9). The selection of these points and exploration strategy are based on digital elevation model (DEM) and digital orthophoto map (DOM) data, which are made from the images obtained by the PCAM at the previous exploration point. Each exploration point is determined after analysis according to the evaluation of its potential scientific outcome. According to the specific working schedule of each scientific payload, a lunar day could be subdivided into several exploration periods. The exploration periods of the lander and rover are also different due to their differing onboard scientific payloads. The LCAM and TCAM of the lander were used only on the first lunar day, while the LFRS and LND work on every lunar day as planned. The exploration periods of each lunar day are divided on the basis of an Earth day (UTC). That is, if 2019-01-03T00:00:00.000 (UTC) to 2019-01-03T23:59:59.000 (UTC) was set as the first exploration period with the number 0001, subsequent numbers are added every Earth day. However, the exploration period of the rover on each lunar day is closely

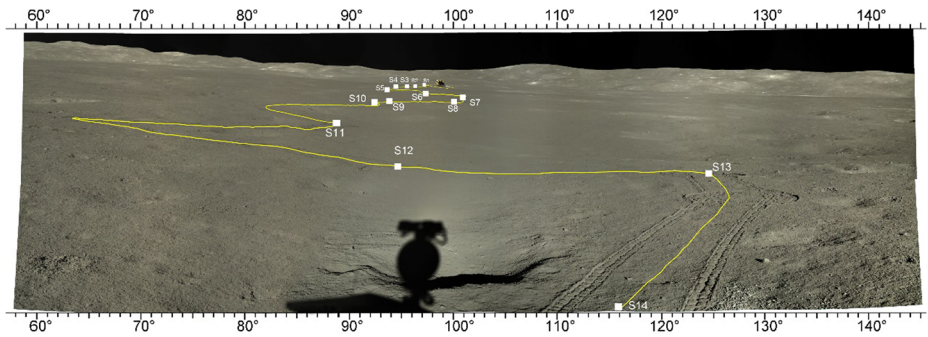


**Fig. 8** The transverse map of the Yutu-2 during the lunar days. The figure shows the rover trace on a image around the landing site which is a mosaic of 13 color lunar images obtained by the right camera of the PCAM. The cylindrical projection is adopted to this image, and the projection median is the yaw axis of the mast of the Yutu-2 rover. The yellow curve shows the rover trace of the Yutu-2, and the white small squares on the trace represent the sleeping position of the rover. Each sleeping position is identified with a letter “S” and an Arabic numeral. “S” refers to sleeping, and the Arabic numeral represents the ordinal number of the lunar day. The azimuth of the lunar surface under the Station Centered Coordinate System (SCCS) is marked with rulers on the top and bottom of the image. The SCCS take the last station position of the rover as the coordinate origin, the local due east and due north directions are +X and +Y axes and the zenith direction is +Z axis. The azimuth angles of 0°, 90°, 180°, and 270°, respectively, represent the due north, due east, due south, and due west of the lunar surface

related to the exploration point. It can be divided into one or more exploration periods according to the actual detection results of the payloads (usually the same as the switch on/off time of the payload). For example, on the second lunar day, there were ten exploration points (LE00201-LE00210); however, they were divided into six periods according to the actual detection situation. Each exploration period includes several exploration points. Thus, the six exploration periods correspond to the point groups LE00201-LE00202, LE00202-LE00204, LE00204-LE00206, LE00206-LE00207, LE00207-LE00208, and LE00208-LE00210. The main exploration activities performed by the payloads on board the rover in the first 14 lunar days are shown in Table 3.

At the end of each lunar day, the obtained payload data are analyzed by the CE-4 Core Scientists Team. Team members are selected from among a wide range of experts from universities and the Chinese Academy of Sciences. Their main task is to plan an observation strategy for the primary mission and future missions and to provide support for the analysis of returned CE-4 scientific data, especially combining the analysis results from multiple instruments comprehensively to advance our understanding of the geological evolutionary history of the lunar far side.

## 5 Data Management

During the exploration periods on each lunar day, each scientific payload obtains specific scientific data, which are packaged according to the Consultative Committee for Space Data Systems (CCSDS) standard and transferred to the ground stations using the Queqiao relay satellite via time-division multiple access (TMDA) through multiple virtual channels (VCs). The ground stations are located in several places, e.g., Miyun (two antennas), Kunming, Kashi, Jiamusi, and South America. The received data are processed by local stations for frame synchronization, descrambling, and Reed-Solomon (RS) decoding to form the frame

**Table 3** List of main exploration activities performed by four scientific payloads of Yutu-2 during the first 14 lunar days

Lunar day	Start time	Exploration point	Rover PCAM	VNIS	LPR	ASAN
1	2019.01.03~2019.01.13	X, A, B, C, D, S1	Take images of the lander at Point A and D with 'Color Mode'; Take a circle shooting at Point S1 with 'Panchromatic Mode'	Take exploration at Point A and S1	Explored along the trace, the exploration distance is 38.1 m	Explored at Point S1
2	2019.01.29~2019.02.11	LE00201~LE00210	Take a circle shooting at Point LE00202, LE00204, LE00206 and LE00208 with 'Panchromatic Mode'; Take two circles shooting at Point LE00210 with 'Panchromatic Mode' and two circle with 'Color Mode'	Explored the rover trace at Point S1, explored the lunar soil at Point LE00202, LE00207 and LE00208	Explored along the trace, the exploration distance is 74.5 m	Explored at Point LE00202 and LE00208
3	2019.02.28~2019.03.13	LE00301~LE00309	Take a circle shooting at Point LE00305, LE00305, LE00308 and LE00309 with 'Panchromatic Mode'	Explored the lunar soil at Point LE00306 and LE00308	Explored along the trace from LE00301 to LE00309, the exploration distance is 42.4 m	Explored at Point LE00303, LE00306 and LE00308
4	2019.03.29~2019.04.12	LE00401, LE00402	Take a circle shooting at Point LE00401 and LE00402 with 'Panchromatic Mode'	Explored the lunar soil with multiple solar azimuth at fixed point at Point LE00401; explored the lunar soil at Point LE00401	Explored along the trace from LE00401 to LE00402, the exploration distance is 14.9 m	Explored at Point LE00401 and LE00402; Explored from multi solar azimuth at fixed point at Point LE00401
5	2019.04.28~2019.05.11	LE00501~LE00506	Take images of the lander at Point LE00501 with 'Color Mode' LE00501; at Point LE00502 and LE00506, take circle shooting with 'Panchromatic Mode' and take images of the lander and mountain in 'Color Mode'	Explored the lunar soil at Point LE00502, LE00504, LE00506 Explored the ejecta of crater at Point LE00505	Explored along the trace from LE00501 to LE00505, the exploration distance is 12.8 m	At Point LE00502, before the lunar noon, facing the sun, explored for 4 hours, after the lunar noon, back to the sun, explored for 1 hour

**Table 3** (Continued)

Lunar day	Start time	Exploration point	Rover PCAM	VNIS	LPR	ASAN
6	2019.05.28~2019.06.09	LE00601~LE00606	Take circle shooting at Point LE00604 and LE00606 with 'Panchromatic Mode'	Explored the lunar soil at Point LE00601~LE00604 and LE00606	Explored along the trace from LE00601 to LE00606, the exploration distance is 19.4 m	Explored at Point LE00601, LE00604 and LE00606
7	2019.06.26~2019.07.09	LE00701~LE00704	Take circle shooting at Point LE00702~LE00704 with 'Panchromatic Mode'; take images of the lander and rover trace at Point LE00704	Explored the lunar soil at Point LE00702 and LE00703	Explored along the trace from LE00701 to LE00704, the exploration distance is 25.8 m	At Point LE00702, before the lunar noon, facing the sun, explored for 4 hours, after the lunar noon, back to the sun, explored for 4 hours; Explored at Point LE00703
8	2019.07.26~2019.08.07	LE00801~LE00806	Take circle shooting at Point LE00803 with 'Panchromatic Mode'; Take images of the crater at Point LE00803 and LE00806	Explored the lunar soil at Point LE00803 and LE00806 Explored the crater boundary at Point LE00804	Explored along the trace from LE00801 to LE00806, the exploration distance is 34.1 m	Explored at Point LE00802, LE00803 and LE00806
9	2019.08.24~2019.09.06	LE00901~LE00912	Take images of the material in the crater pit at Point LE00901, LE00904~LE00906 with 'Color Mode'; Take images of the crater and rover trace at Point LE00912 with 'Color Mode'	Explored the lunar soil around the crater, ejecta of the crater and lunar soil from the inner crater at Point LE00901~LE00911	Explored along the trace through LE00901, LE00905, LE00906 to LE00912, the exploration distance is 13.8 m	Explored at Point LE00905
10	2019.09.22~2019.10.05	LE01001	Take circle shooting at Point LE01001 with 'Color Mode'	Explored the lunar soil at Point LE01001 with multiple solar azimuth at fixed point	Explored along the trace, the exploration distance is 4.9 m	Explored from multi solar azimuth at fixed point

**Table 3** (Continued)

Lunar day	Start time	Exploration point	Rover PCAM	VNIS	LPR	ASAN
11	2019.10.22~2019.11.04	LE01101~LE01105	Take circle shooting at Point LE01103 and LE01105 with 'Panchromatic Mode'	Explored the lunar soil at Point LE01102 and LE01103	Explored along the trace, the exploration distance is 31.3 m	Explored at Point LE01102 and LE01103
12	2019.11.21~2019.12.04	LE01201~LE01205	Take circle shooting at Point LE01203 with 'Panchromatic Mode'; take images of crater and rock at Point LE01205 with 'Color Mode'	Explored the lunar soil at Point LE01203	Explored along the trace, the exploration distance is 28.3 m	Explored at Point LE01203
13	2019.12.20~2020.01.02	LE01301~LE01311	Take images of 18 m crater at Point LE01301 with 'Color Mode'; Take circle shooting at Point LE01304 with 'Panchromatic Mode'; take images of the rock at Point LE01311 with 'Color Model'	Explored the rock at Point LE01302, LE01303, LE01306, LE01307 and LE01310	Explored along the trace through LE01301, LE01304, LE01308, LE01309 to LE01311, the exploration distance is 8.1 m	Explored at Point LE01304 and LE01308
14	2020.01.18~2020.02.01	LE01401, LE01402	Take images of the rock and rover trace at Point LE01401 with 'Color Model'; Take circle shooting at Point LE01402 with 'Panchromatic Mode' and take images of lander, rover trace, crater and rock with 'Color Mode'	Explored the lunar soil at Point LE01402	Explored along the trace, the exploration distance is 13.4 m	At Point LE01402, before the lunar noon, facing the sun, explored for 4 hours, after the lunar noon, back to the sun, explored for 4 hours

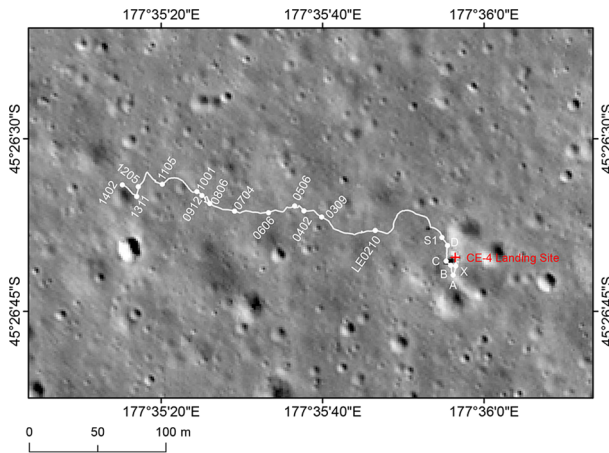


**Fig. 9** Rover trace and exploration points of the Yutu-2 for 14 lunar days. The white dot on the rover trace is the exploration point, which is identified by “LE” and five following numerals. These numbers are composed of lunar day serial number (the former 3 digits) and the exploration point serial number (the latter 2 digits). For example, LE00201 represents the first exploration point (01) of the second lunar day (002). “LE0” is omitted for the abbreviation. LRO NAC (Narrow Angle Camera) image, M1303619844, is used as the base image, with a resolution of 1.4 m

data. The frame data are then transmitted to the Ground Application and Research System (GRAS) headquarters in Beijing, and preprocessing on the received frame data is performed to yield standard Level 0, 1, and 2 data products for each scientific payload (for the detailed processing methods, see Li et al. 2015). The data of all levels are submitted to the data management system for archiving and then released according to the administrative procedures issued by the CNSA. A schematic diagram of the data flow is shown in Fig. 10.

## 5.1 Data Archiving

Data quality is the basic guarantee for the correctness, validity, and availability of scientific data. For the specialized data resources related to each scientific payload, a data quality system is established by the principal investigator. The data are inspected by specialized teams via a comprehensive set of procedures, including ground tests, processing method design and optimization, verification of data correctness, and evaluation of the data quality. The data meeting the requirements of these inspections are then submitted for archiving.

The data archiving team is responsible for preparing the data, performing data archiving and checking and verifying the consistency, standardization, integrity, and completeness of the data according to the established standards and specifications. They also perform unified standardized processing to establish datasets organized by their attributes, such as exploration missions, scientific payloads, data types, and processing levels, and provide refined management in terms of time, space, format, and quality. At the same time, they establish localized multicopy backups of the data and remote replications of the core datasets for effective archiving, secure storage, and permanent preservation of the datasets. From the CE-4 mission, the preprocessed standard data products (Level 0 to Level 2) of each scientific payload are organized in PDS4 format. Each data product is composed of a data file in PDS format and a descriptive label file in XML format. Table 4 shows the main archived data products of the CE-4 mission.



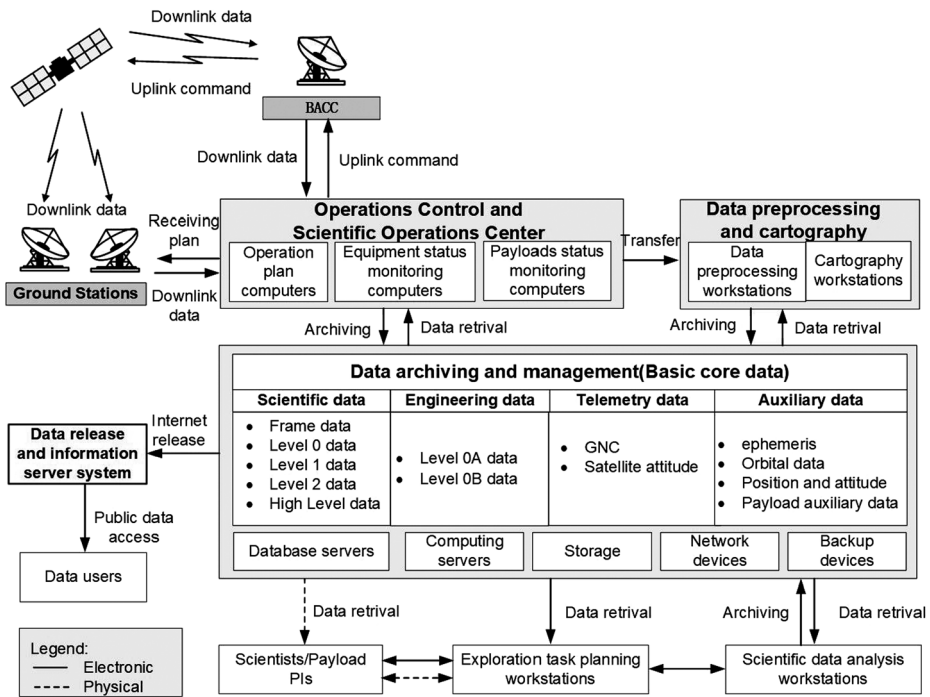


**Fig. 10** The schematic of GRAS emphasizing the data flow through the system

## 5.2 Data Accessibility

After the successful landing of the CE-4 probe on January 3, 2019, the payloads began to acquire data. The GRAS completed the processing of the downlinked scientific data to generate the Level 0B product within one month. According to the administrative data release procedures issued by the CNSA, scientific data have been released to specific users through offline copying since February 2019. First, the data were provided to payload development units for probe and payload in-flight testing, instrument performance analysis, and data processing method improvement to provide decision support for the probe's in-flight status and for the verification and adjustment of the payload status. Second, scientific data acquired by the various payloads are released to a designated scientific research panel. As of January 2020, the GRAS released preliminary scientific data acquired by the nine payloads to more than 100 scientists on the scientific research panel after the end of each lunar day. In total, 17,703 data files with a size of 37.7 GB were immediately delivered in 12 batches. On April 18, 2019, the CNSA organized the first batch of scientific data handover ceremony in Beijing for the CE-4 international payloads, distributing the scientific data of the ASAN, LND instrument, and NCLE to Sweden, Germany, and the Netherlands, respectively. Afterward, the updated exploration data acquired by international payloads were released monthly.

Following the administrative procedures, the GRAS publicly released the CE-4 data through the website <http://moon.bao.ac.cn> to global users for the first time on January 3, 2020, including the scientific data products of the first and second lunar days acquired by the five scientific payloads on board the lander and rover (a total of 12,512 files with a size of 10.5 GB, Table 5). The link to access these data is <http://moon.bao.ac.cn/pubMsg/detail->

**Table 4** The CE-4 data products

Instrument	Instrument data product	Description	Data format
LCAM	Raw LCAM data	LCAM source packet data and data blocks by LCAM generated, include Level 0A and Level 0B data products	Binary package
	LCAM Standard Data Products	Lunar images continuously acquired by the landing camera during the soft landing phase, including Level 01, Level 2A and Level 2B data products	PDS4
	Landing images	5441 Images acquired by the landing camera	jpg
	Landing videos	Videos acquired by the landing camera	MP4
TCAM	Raw TCAM data	TCAM source packet data and data blocks by TCAM generated, include Level 0A and Level 0B data products	Binary package
	TCAM Standard Data Products	360° topographical data obtained by the TCAM, including Level 01, Level 2A, Level 2B and Level 2C data products	PDS4
	Images taken by the Lander and Rover, respectively	Images for the the rover	jpg
	Panoramic mosaic image of landing site surface	Panoramic mosaic images under cylindrical projection and azimuthal projection using 360° image data	jpg
LFRS	Raw LFRS data	LFRS source packet data and data blocks by LFRS generated, include Level 0A and Level 0B data products	Binary package
	LFRS Standard Data Products	Solar low frequency radio and lunar low frequency radiation environment observation data, including Level 01, Level 2A, Level 2B and Level 2C data products	PDS4
LND	Raw LND data	LND source packet data and data blocks by LND generated, include Level 0A and Level 0B data products	Binary package
	LND Standard Data Products	Lunar surface energy neutral particles (neutron and gamma rays) and charged particles radiation environment detection data, including Level 01 and Level 2A data products	PDS4
PCAM	Raw PCAM data	PCAM source packet data and data blocks by PCAM generated, include Level 0A and Level 0B data products	Binary package
	PCAM Standard Data Products	The topographical data of lunar surface at the exploration points, including 360° panchromatic and color images, and color images of the landers, craters, rocks, ejected materials, including Level 01, Level 2A, Level 2B and Level 2C data products	PDS4
	Images taken by the Lander and Rover, respectively	Images for the Lander	jpg
	Panoramic mosaic images of exploration points	Panoramic mosaic images under cylindrical projection and azimuthal projection using 360° image data	jpg

**Table 4** (Continued)

Instrument	Instrument data product	Description	Data format
LPR	Raw LPR data	LPR source packet data and data blocks by LPR generated, include Level 0A and Level 0B data products	Binary package
	LPR Standard Data Products	Detection data of shallow structures in the roving area, i.e., radar echoes acquired by the first and second channel, including Level 01, Level 2A and Level 2B data products	PDS4
VNIS	Raw VNIS data	VNIS source packet data and data blocks by VNIS generated, include Level 0A and Level 0B data products	Binary package
	VNIS Standard Data Products	Material composition detection data, i.e., visible near-infrared spectral image data, short-wave infrared spectral data, and single-point spectral data, including Level 01, Level 2A and Level 2B data products	PDS4
ASAN	Raw ASAN data	ASAN source packet data and data blocks by ASAN generated, include Level 0A and Level 0B data products	Binary package
	ASAN Standard Data Products	Detection data of energy neutral atoms and positive ions on the lunar surface in the roving area, including Level 01, Level 2A and Level 2B data products	PDS4
NCLE	Raw NCLE data	NCLE source packet data and data blocks by NCLE generated, include Level 0A and Level 0B data products	Binary package

[CE4EN.jsp](#). The CE-4 images and videos were also released on the multimedia database platform at <http://moon.bao.ac.cn/mul/index/list>. The updated data will be published periodically and incrementally over a certain amount of time.

## 6 Preliminary Results

Due to the complex terrain of the lunar surface along the transverse path of the lander, the CE-4 probe adopted a near-vertical descent approach (Sun et al. 2019), in which the probe was adjusted to a descent path almost vertical to the surface of the Moon in a very short time after the beginning of the powered descent phase. This process is different from the smooth parabola-like landing of CE-3. The LCAM was the first payload to be powered on the probe. It started operating 5 minutes and 11 seconds after the powered descent phase and took images of the soft-landing process every second. In the end, it captured 5441 images, describing the topography and morphology near the landing area with resolutions ranging from meters to hundreds of kilometers (Fig. 11). These images also provided a basis for the reconstruction of the powered descent trajectory, the precise positioning of the landing site, and the precise topographic analysis of the landing area.

One hundred eighty sequence images were selected from the image data obtained by the LCAM, and 30,992 homologous points were extracted as the connections between these images, which also restored the relative positions of the cameras at the time the images were taken. Moreover, 12 plane control points and one elevation control point were selected based on the high-resolution topographic data product (CE2TMAP2015). Then, the exterior

**Table 5** List of the first batch of the CE-4 scientific data products released publicly (including some scientific payloads exploration data acquired during the first and second lunar day)

Instrument	Lunar day	Data level	Data product description	Files	Volume (MiB)
LCAM	1	Level 2A	Images of the landing site, including 5358 images with 8:1 compression ratio and 83 images with 64:1 compression ratio, and their corresponding descriptive label files	10882	5461.6
TCAM	1	Level 2C	240 color images, and the 240 corresponding descriptive label files	480	2764.8
PCAM	1	Level 2B	124 panoramic images, 50 color images, and their corresponding descriptive label files	348	629.0
	2	Level 2B	338 panoramic images, 6 color images, and their corresponding descriptive label files	688	703.6
LPR	1	Level 2B	Radar echoes data acquired by the first channel, the second channel antenna A and the second channel antenna B during the three exploration periods, and their corresponding descriptive label files	18	363.4
	2	Level 2B	Radar echoes data acquired by the first channel, the second channel antenna A and the second channel antenna B during the six exploration periods, and their corresponding descriptive label files	36	560.3
VNIS	1	Level 2B	Imaging spectral data (calibration data) and single-point spectral data (detection data) of visible near-infrared and short-wave infrared bands at two detection points, as well as their corresponding descriptive label files and auxiliary files.	20	100.1
	2	Level 2B	Imaging spectral data (calibration data) and single-point spectral data (detection data) of visible near-infrared and short-wave infrared bands at four detection points, as well as their corresponding descriptive label files and auxiliary files.	40	200.3

orientation elements (position and attitude) of each LCAM image and the corresponding lunar coordinates of the image points were calculated by the bundle adjustment method. On this basis, the high-precision topography of the CE-4 landing site was reconstructed with photogrammetry. The 5-cm-resolution DOM (CE4DOM2019) and DEM (CE4DOM2019) data of the landing site were produced (Liu et al. 2019), as shown in Fig. 12. The standard deviations of the position and elevation errors are 0.715 m (1 $\sigma$ ) and 1.040 m (1 $\sigma$ ), respectively. According to these results, it was finally confirmed that the landing site of CE-4 was (45.4446° S, 177.5991° E), with an elevation of -5935 m (Liu et al. 2019). See the point marked with the “+” symbol in Fig. 12.

As shown in Fig. 12(a), a large number of craters with diameters ranging from tens of centimeters to tens of meters are distributed around the CE-4 landing site. Several craters surrounding the landing site have small diameters and shallow depths, as depicted in Fig. 12(b). The landing site is relatively flat, with the eastern side showing a relatively higher elevation than the western side.

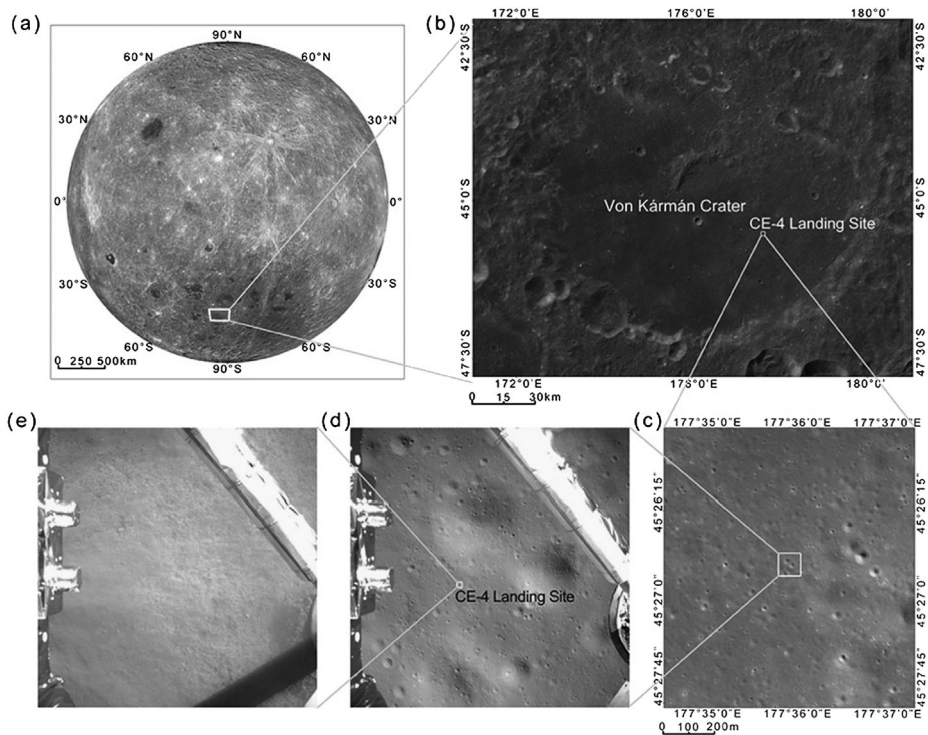


**Fig. 11** Positioning the CE-4 landing site with the lunar images: (a) Von Kármán Crater in lunar far side, a map made with Chang'e-2 DOM (50 m resolution); (b) the CE-4 landing site in Von Kármán Crater, a map made with Chang'e-2 DOM (7 m resolution); (c) the CE-4 landing site in Von Kármán Crater, a map made with CE-4 landing camera (2 m resolution); (d) Image captured when lander hovering above the landing site at a height of 100 meters (8 cm resolution); (e) Image captured when lander touched the Moon (1 mm in resolution) at 10:25:54 (UTC+8) on January 3, 2019

After the confirmation of the precise location of the CE-4 landing site on the Moon, the nomenclature of the landing site and its surrounding features were determined. On February 4, 2019, the IAU approved the five lunar feature names requested by the GRAS: Statio Tianhe for the CE-4 landing site; Zhinyu, Hegu, and Tianjin for the three small craters arranged in a triangle near the landing site, and Mons Tai for the central peak inside the Von Kármán crater (IAU WGPSN 2019) (Fig. 13).

The TCAM is a color camera installed on the mast of the CE-4 lander. Its focal length is 43 mm, its field of view is  $22.9^\circ \times 16.9^\circ$ , and its detector size is  $2352 \times 1728$ . It can capture images with azimuth angles and pitch angles ranging from  $0^\circ$  to  $360^\circ$  and  $-60^\circ$  to  $+60^\circ$ , respectively. The TCAM was designed to perform topography surveys around the landing site on only the first lunar day. It completed the tasks of acquiring images of the rover and building panoramas of the full scene around the landing site. The TCAM built the first panoramas of the lunar surface with 320 images taken from eight pitch angles of  $0^\circ$ ,  $-15^\circ$ ,  $-30^\circ$ ,  $-45^\circ$ ,  $-60^\circ$ ,  $3^\circ$ ,  $-5.9^\circ$ ,  $-5.9^\circ$  when the rover was at Point A. The second panoramas of the lunar surface were built according to 120 images taken from three pitch angles (i.e.,  $0^\circ$ ,  $-15^\circ$  and  $-30^\circ$ ) when the rover was at Point D. These two panoramas cover the entire path of the rover from Point A to Point D. The panoramic mosaic image of the CE-4 landing site was generated after radiometric correction, color restoration, and image mosaicking

**Fig. 12** Image and topography map of the CE-4 landing site made by using DOM (a) and DEM (b) data

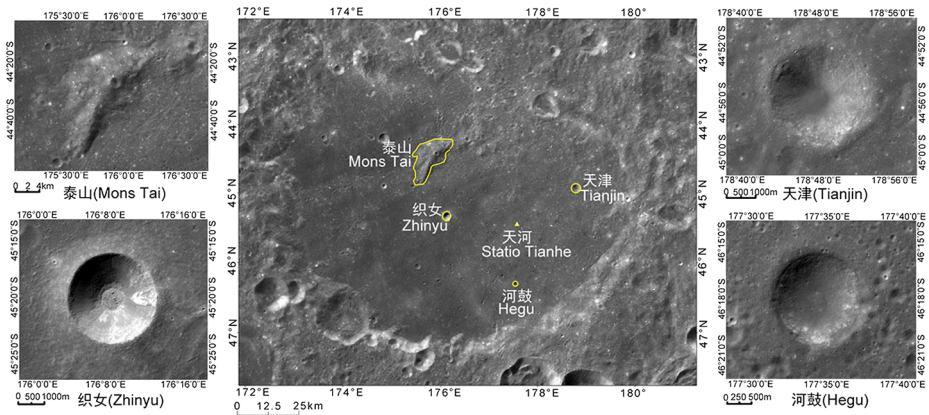
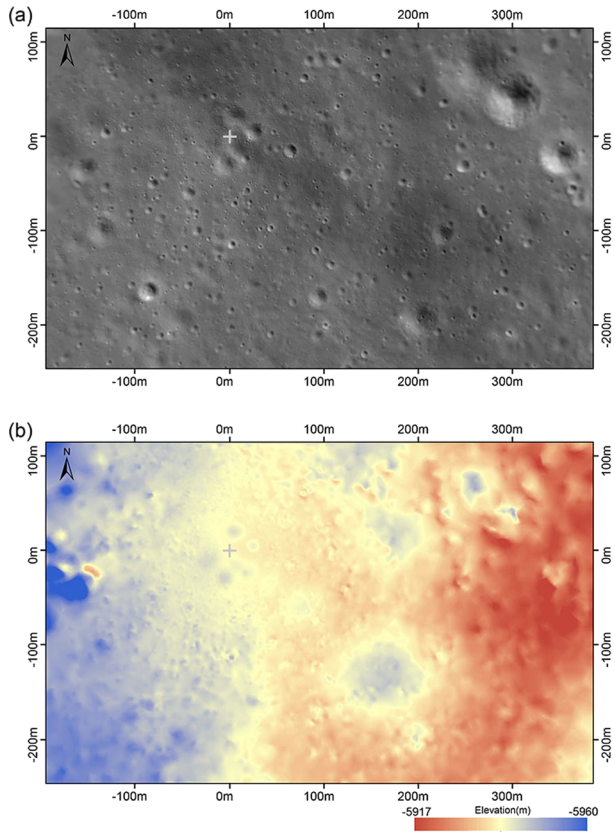


**Fig. 13** Overview of the CE-4 landing area and the feature names

(Fig. 14). It can be seen from the color images of the TCAM that there are a number of small craters and a large amount of dark, fine-grained soil materials without many large rocks around the CE-4 lander, which is different from what was observed around the CE-

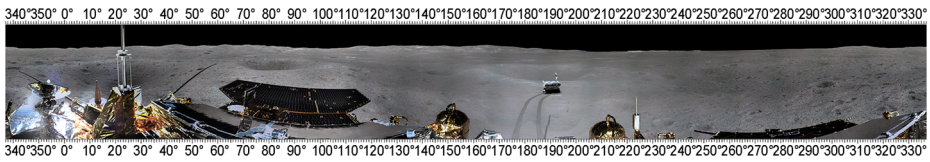


**Fig. 14** The panoramic mosaic image of the lunar surface is obtained by the TCAM. This image is made of 60 lunar color images in three circles (20 images per circle), which are shot by TCAM at pitch angles of  $0^\circ$ ,  $-15^\circ$ , and  $-30^\circ$ . The cylinder projection method is adopted. The center axis of the cylinder is the yaw axis of the camera pointing mechanism. The azimuth of the lunar surface under the SCCS is marked with rulers on the top and bottom of the image

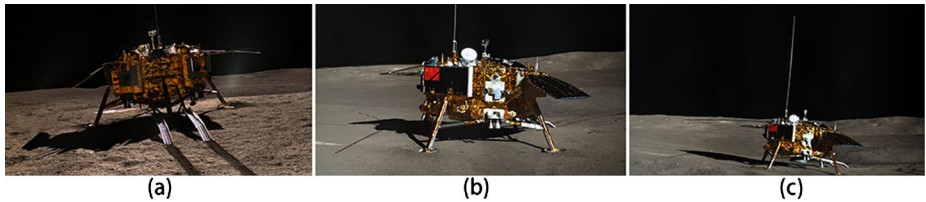


**Fig. 15** Mosaic of the lander taken by PCAM. (a–c), the images of the lander taken at Point A, Point D, and Point S1, respectively. Each picture is a mosaic of six images taken at different angles

3 landing site (Xiao 2014). The lunar soil is brighter close to the lander, which may have resulted from relatively fresh lunar soils exposed by the engine plume of the lander. The rover was located south of the lander in the image taken by the TCAM and adjacent to a crater, whose surrounding reflectivity is higher than that of other areas. Some fragmental impact debris can be seen on the rim of this crater. After the rover passes through, two apparent dark wheel tracks can be observed on the lunar surface. Along the rover's path, towards the far horizon, an undulating mountain-like structure could be seen, which might be the south wall of the Von Kármán crater.

During the first lunar day, the PCAM took color images of the lander when the rover reached exploration Points A, D, and S1. Since the rover was close to the lander at those points, only one image acquired by the PCAM cannot cover the whole lander because of the limitation of its field of view. Therefore, the PCAM rotated six times at each detection point to take six images of the lander from different angles. These images were then processed and mosaicked to form the whole image of the lander (Fig. 15). The PCAM also took a number of images of the lunar surface at Point S1 and built a panoramic image around the landing point (Fig. 16). There are many large and small impact craters close to the landing site. A relatively large and deep crater is located in front of the lander (i.e., to the northeast of the lander). In the following exploration, the PCAM obtained the image of the lunar surface around each exploration point in the transverse path according to the exploration plan. This image is critical for terrain analysis and scientific exploration planning. By the end of the 14th lunar day, the PCAM had already worked for 61.3 hours and obtained 28 panoramic mosaics, 227 pairs of color images and 1195 pairs of panchromatic stereo images. The GRAS used these stereo images to restore the topography around the exploration point, where the rover is located. Stereo images of each exploration point were also produced. Lunar far-side images captured by the TCAM and PCAM provide the first opportunity to investigate the geomorphology and topography of the deepest, largest, and oldest impact basin on the far side of the Moon.

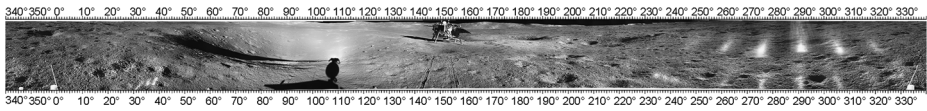


**Fig. 16** Mosaic of panchromatic images of the lunar surface taken by PCAM at S1. This mosaic was generated by the two panoramas (28 images per panoramas) captured by the PCAM at Point S1 on January 12, 2019, with pitch angles of  $-7^\circ$  and  $-19^\circ$  (corresponding to camera pointing mechanism). The cylindrical projection method is adopted, and the central axis of the cylinder is the yaw axis of the mast of the lunar rover. The azimuth of the lunar surface under the SCCS is marked with rulers on the top and bottom of the image

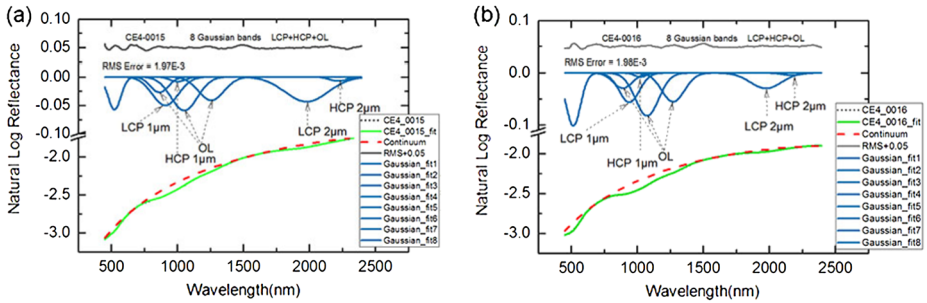


**Fig. 17** The CE-4 reflectance spectra acquired by the VNIS during the first lunar day. MGM (Modified Gaussian Model) fitting results for the CE4\_0015 at exploration point A (a) and the CE4\_0016 at exploration point S1 (b) using endmembers of low-Ca pyroxene, high-Ca pyroxene, and olivine. (Li et al. 2019a)

The VNIS acquires reflectance data of the landing site between 450 and 2400 nm with spectral resolutions varying from 2.4 to 6.5 nm for the hyperspectral imaging detector (VIS/NIR, 450~950 nm) and from 3.6 to 9.6 nm for the single-point spectrometer (SWIR, 900~2400 nm). The VNIS enabled the first in situ measurements of the composition of the lunar surface materials along the traverse path of the rover. The analysis results from the VNIS data acquired at Points A and S1 during the first lunar day suggest that the materials of the landing site are quite different from the collected lunar mare basalts. These materials are mainly composed of mafic components dominated by olivine and low-Ca pyroxene with only a small amount of high-Ca pyroxene (Fig. 17). This mineral combination could represent the mantle material excavated and ejected to the floor of the Von Kármán crater by the Finsen impact crater event (Fig. 18, Li et al. 2019a). Alternatively, recent analysis shows that the lunar soil within the landing site is mainly composed of plagioclase, olivine, low-Ca pyroxene, and a small amount of high-Ca pyroxene. The rock type is more similar to olivine-norite originating from the lower crust or crystallizing from the impact-derived melt pool formed by the SPA impact event (Hu et al. 2019; Lin et al. 2019; Ling et al. 2019). These results provide new constraints on the depth and cooling rate of the early magmatic ocean and are of significant importance in exploring the early evolutionary history of the Moon.

The CE-4 LPR is a dual-frequency GPR system that operates at 60 MHz (low frequency) and 500 MHz (high frequency), corresponding to ranges of 40 to 80 MHz and 250 to 750 MHz, respectively. The LPR ran 49.8 hours until the end of the 14th lunar day, and its effective exploration distance was approximately 367.3 m. The data on 36,611 low-frequency channels and 158,434 high-frequency channels were obtained.



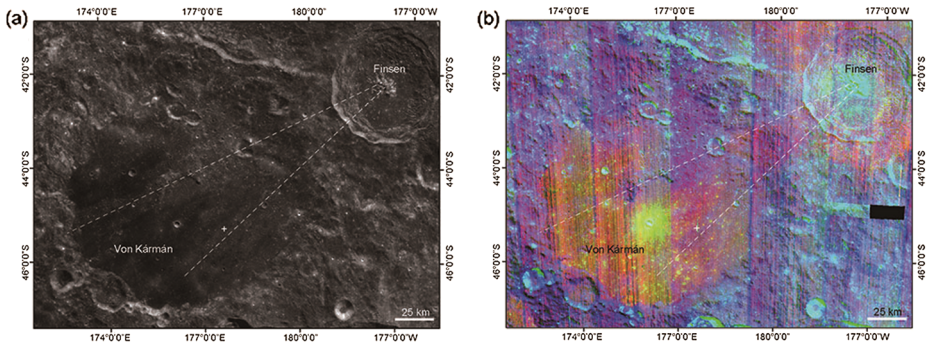


**Fig. 18** Distribution of Finsen ejecta in the Von Kármán crater. (a) CE-1 DOM, spatial resolution 120 m; (b) M3 hyperspectral data color composite. White dashed lines represent two major northeast-southwest ejecta rays of the Finsen crater converging towards its central peak. White cross is the Chang'e-4 landing site, which is located on the ejecta material of the Finsen crater. (Li et al. 2019a)

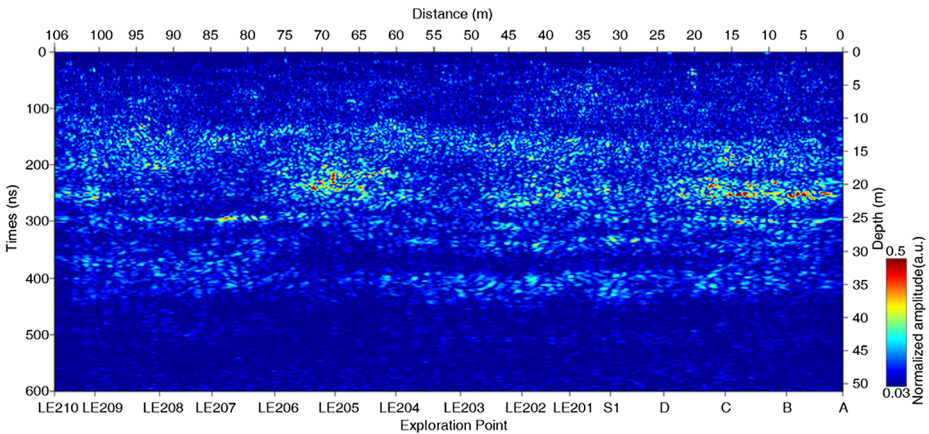


**Fig. 19** Tomographic reconstruction of the radar data; red, high reflectivity (large electromagnetic contrast); blue, low reflectivity (small electromagnetic contrast). (Li et al. 2020)

The analysis results of the LPR data for the first two lunar days indicated that the signal penetration at the CE-4 landing site is much greater than that at the CE-3 landing site. This finding means that the attenuation of radar waves by subsurface materials in the CE-4 landing area is much smaller than expected (Fig. 19). Further analysis showed that the subsurface around the CE-4 landing site has three different units (Fig. 20), which were probably formed by ejected deposits from several large craters, such as Finsen, at different times. It is speculated that the material resulting in easy penetration of radar waves is plagioclase-gabbro rather than basalt (Li et al. 2020). This result reveals a very complex volcanic and impact history at the CE-4 landing site.

The two main scientific objectives of the LFRS experiment include the detection of solar bursts and the detection of radio background spectra at the CE-4 landing site. The operating frequency of the LFRS is from 10 kHz to 40 MHz, which is divided into a low-frequency band (from 10 kHz to 2 MHz) and a high-frequency band (from 1 MHz to 40 MHz). The LFRS consists of three 5-m-long orthogonal monopole antennas, which are mounted on the

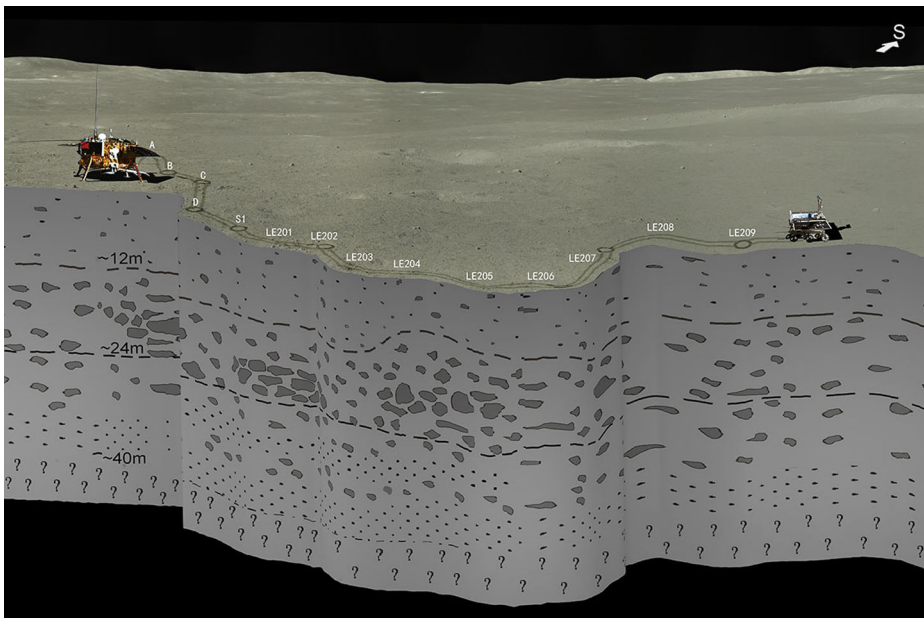
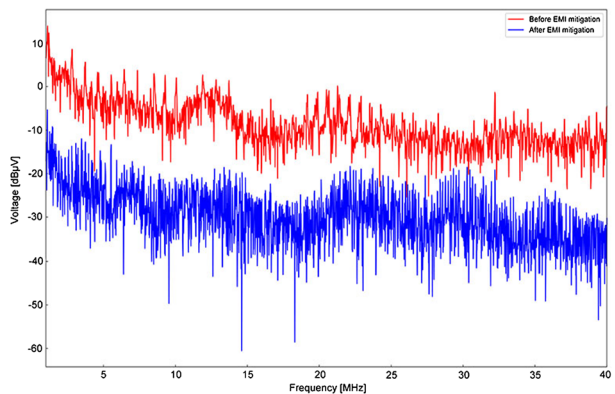


**Fig. 20** The schematic representation of the subsurface geological structure at the CE-4 landing site inferred from LPR observations. The subsurface can be divided into three units: Unit 1 (up to 12 m) consists of lunar regolith, Unit 2 (depth range, 12–24 m) consists of coarser materials with embedded rocks, and Unit 3 (depth range, 24–40 m) contains alternating layers of coarse and fine materials

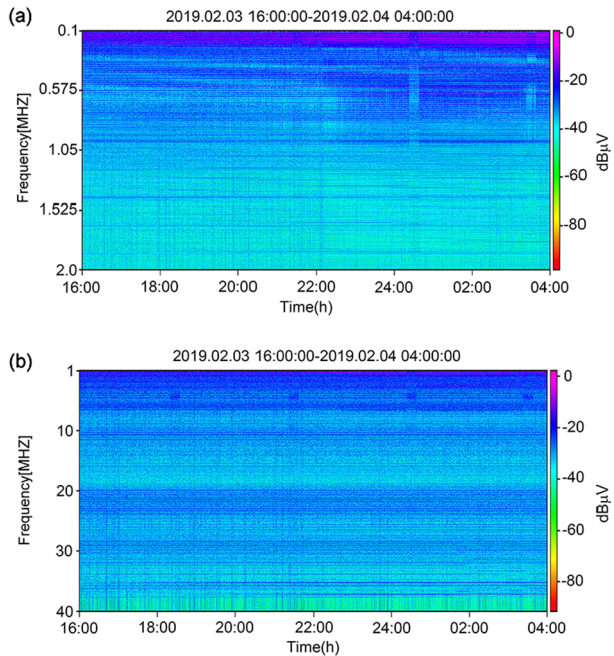
**Fig. 21** A comparison result before and after EMI mitigation



bottom of the CE-4 lander, to receive signals in all polarization states. A new method to suppress electromagnetic interference (EMI) from the lander employs another short antenna with a length of 20 cm. From Fig. 21, the EMI could be reduced by ~15 dB after mitigation. By the end of the 14th lunar day, the LFRS obtained a total of 1018.3 hours of observation data. The primary results are shown in Fig. 22. Further calibration and analysis are needed.

The LND instrument measures the radiation dose and the neutron flux of charged and neutral particles and detects the radiation environment of high-energy charged particles on the lunar surface. By the end of the 14th lunar day, the LND instrument had operated for 3435.2 hours. Preliminary analysis of the LND data obtained during the first and second

**Fig. 22** The time-frequency spectrogram received by one antenna of LFRS after EMI mitigation at low frequency (a) and high frequency (b)



lunar days shows an average total dose rate in silicon of  $13.2 \pm 1 \mu\text{Gy}/\text{hour}$  and a neutral particle dose rate in silicon of  $3.1 \pm 0.5 \mu\text{Gy}/\text{hour}$ . The background due to the RTG and RHUs was measured on the ground, and the values reported above have been corrected accordingly. By subtracting the neutral contribution, the result shows that the average absorbed dose rate due to charged particles is  $10.2 \pm 1.1 \mu\text{Gy}/\text{hour}$  in silicon (Fig. 23). The LND measurements are basically consistent with the measured result of the Cosmic Ray Telescope for the Effects of Radiation (CRaTER) on the Lunar Reconnaissance Orbiter (LRO), and the radiation dose rate decreases with decreasing orbital height, following the change trend in the radiation dose in the lunar space environment (Mazur et al. 2011; Zhang et al. 2020a).

The ASAN, which is on board the Yutu-2 rover, measures the energy and components of neutral atoms as well as positive ions within the range of  $10 \text{ eV} \sim 10 \text{ keV}$ . By the end of the 14th lunar day, it had taken 53.6 hours to measure the neutral atoms and positive ions at the landing site. The scientific data reflected the distribution of neutral atoms and positive ion fluxes at different solar azimuths and incident angles. The cutoff energy of energy-neutral particles exhibited a strong correlation with the velocity of the incident solar wind. The preliminary analysis of the corresponding mass spectra revealed that neutral hydrogen is the dominant component (Wieser et al. 2019). The reflectivity of neutral hydrogen with energy greater than 30 eV is approximately 32% on the surface of the Moon, which is compatible with what was observed from orbit by Chandrayaan-1 and the Interstellar Boundary Explorer (IBEX) (Wurz et al. 2009; Wieser et al. 2010, 2019; Zhang et al. 2020b), but the flux of low-energy neutral particles is higher than those observed by Chandrayaan-1 and IBEX (Fig. 24).

## 7 Summary

The CE-4 lander, rover and relay satellite with nine scientific payloads performed exploration tasks over 14 lunar days according to a predefined exploration plan. They obtained a

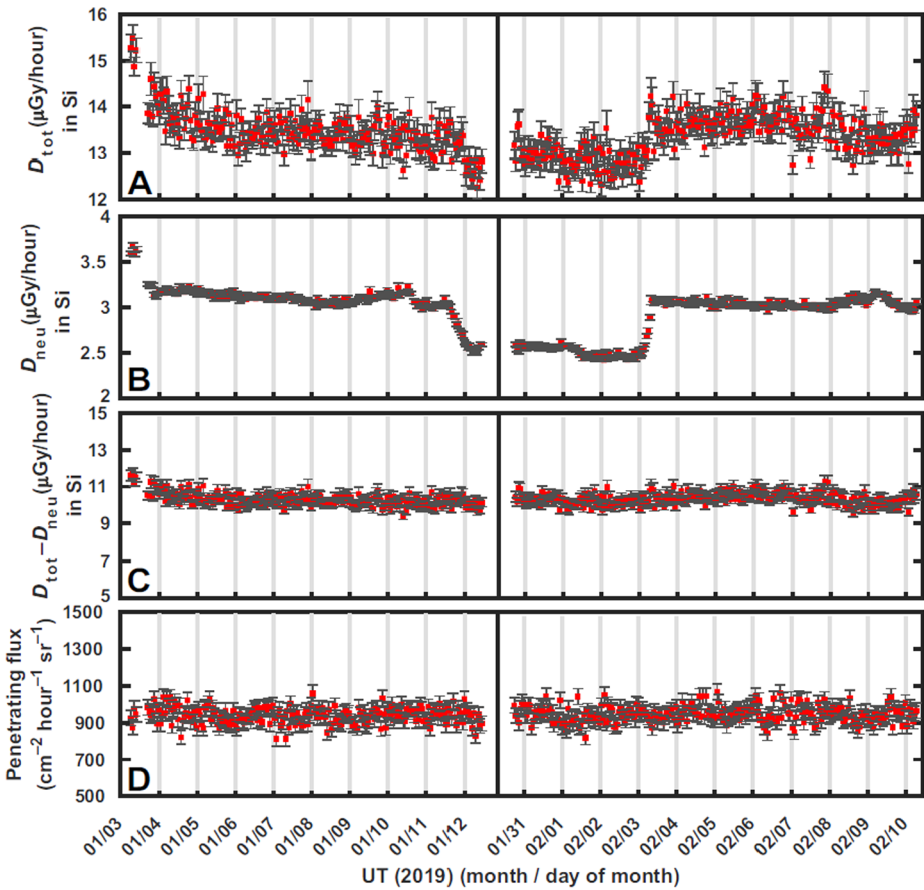


**Fig. 23** Temporal evolution of the radiation environment on the Moon as measured by LND on Chang'E 4 during the first and second lunar day after Chang'E4 landed. The left-hand panels show data for the first lunar day, and the right-hand panels show data for the second lunar day. **(A)** Total absorbed dose rate measured with the LND B silicon detector. **(B)** Neutral particle dose rate recorded in the LND C1 silicon detector. **(C)** Total absorbed dose rate from charged particles only [i.e., (A and B)]. The known background from the RTG and RHUs (20) has been subtracted from the values reported in (A) and (B). **(D)** Temporal evolution of the flux of penetrating particles. UT, universal time (Zhang et al. 2020a)

batch of original data, and some preliminary analysis results of these data were acquired. In the follow-up exploration plan, the payloads will continue to conduct low-frequency radio-astronomical observations, mineral composition and shallow structure detection, neutron and radiation dose as well as energy-neutral atom detection on the far side of the Moon. These detections are expected to provide new data for radio-frequency astronomical observations within the range of 0.1 to 1 MHz and to establish the first comprehensive geological profile and evolutionary model that integrates the topography, shallow structure, and composition of the lunar far side, advancing our understanding of the evolutionary history of the Moon and the universe.

CE-4 is the first successful mission that achieved a soft landing and performed rover reconnaissance on the lunar far side. The scientific outcome and technical experience obtained in this mission will lay a solid foundation for the Chang'e-5 mission, which will be launched

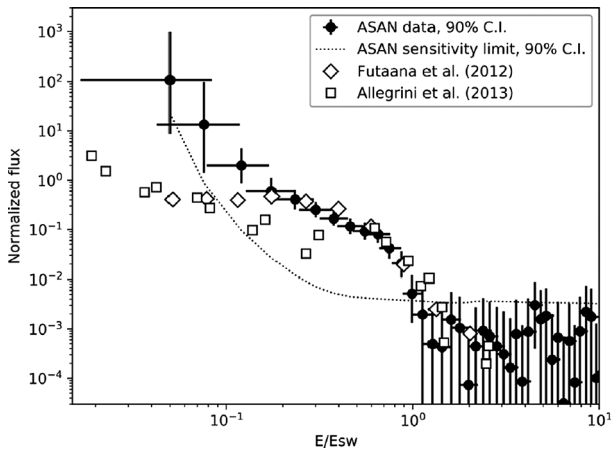


**Fig. 24** Solid circles: Average hydrogen ENA energy spectrum observed by the ASAN on 2019/5/1 06:18–10:45 UTC, normalized to the solar wind energy  $E_{sw}$ . Vertical error bars correspond to 90% confidence limits (C.I.) (Feldman and Cousins 1998), horizontal error bars correspond to the full width at half maximum of the energy response. The dotted line represents a 90% confidence limit, below which the ASAN signal cannot be distinguished from the case where no signal is present. Open diamonds: Hydrogen ENA energy spectrum observed by SARA on Chandrayaan-1 from (Futaana et al. 2012), again normalized to the solar wind energy. Open squares: Sample hydrogen ENA spectrum measured by IBEX (Allegrini et al. 2013), normalized in the same way (Zhang et al. 2020b)

by the end of 2020, and follow-up exploration missions, such as Chang'e-6, Chang'e-7, and Chang'e-8, aimed at the lunar south pole region around 2030 (Li et al. 2019b). The international payloads of CE-4 are the comprehensive cooperation between China and international research institutions in the fields of lunar scientific exploration mission planning and data acquisition, processing, and sharing. The acquired data deepen our understanding of the lunar environment, cosmic space, and solar activity. CE-4 is an exploration mission that brings about not only scientific outcomes but also concrete practice for building a community of a shared future for humankind. China will work with the international community to make greater contributions to promote human civilization and progress.

**Acknowledgements** This research was supported by the Chang'E-4 mission of the Chinese Lunar Exploration Program (CLEP) and the National Natural Science Foundation of China (No.41671458). We thank the team members of the Ground Research and Application System (GRAS), who have contributed to data receiving, preprocessing, management and release.

**Authors' contributions** C.L.L., W.Z., and W.W.B. designed the work, performed data analysis, and wrote the manuscript. X.G.Z., X.Y.G., Y.X.L., Q.F., Y.S., X.R., F.W., D.W.L., B.L., and Z.Y. OY processed and analyzed the payload data. Z.B.Z., J.J.L., W.Y., X.T., and H.B.Z. contributed to data receiving, data preprocessing, data management, and instrument operations.

**Data availability** Not applicable.

**Code availability** Not applicable.

**Conflicts of interest/Competing interests** The authors declare that they have no known competing financial interests or personal relationships that could have appeared to influence the work reported in this paper.

**Publisher's Note** Springer Nature remains neutral with regard to jurisdictional claims in published maps and institutional affiliations.

## References

- F. Allegrini, M.A. Dayeh, M.I. Desai, H.O. Funsten, S.A. Fuselier, P.H. Janzen, D.J. McComas, E. Möbius, D.B. Reisenfeld, M.D.F. Rodríguez, N. Schwadron, P. Wurz, Lunar energetic atom (ENA) spectra measured by the interstellar boundary explorer (IBEX). *Planet. Space Sci.* **85**, 232–242 (2013). <https://doi.org/10.1016/j.pss.2013.06.014>
- M.J. Arts, D.S. Prinsloo, M. Ruiters, A.J. Boonstra, Design of a reconfigurable array of monopoles for the Netherlands China Low-frequency Explorer, in *2019 13th European Conference on Antennas and Propagation (EuCAP)*, Krakow, Poland (2019), pp. 1–5
- S. Bandyopadhyay, J. Lazio, A. Stoica, P. Goldsmith, B. Blair, M. Quadrelli, J.P. de la Croix, A. Rahmani, Conceptual ideas for radio telescope on the far side of the Moon, in *2018 IEEE Aerospace Conference*, Big Sky, MT, USA (2018), pp. 1–10. <https://doi.org/10.1109/AERO.2018.8396801>
- J.P. Basart, J.O. Burns, A very low frequency array for the lunar far-side, in *Lecture Notes in Physics*, vol. 362 (1990), pp. 52–56. [https://doi.org/10.1007/3-540-52891-1\\_107](https://doi.org/10.1007/3-540-52891-1_107)
- P.-Y. Bely, R.J. Lurance, S. Volonte, R.R. Ambrosini, A. van Ardenne, C.H. Barrow, J.-L. Bougeret, J.-M. Marcaide, G. Woan, Very low frequency array on the lunar far side. Technical Report. ESA SCI (97).2 (1997)
- A. Boonstra et al., Discovering the sky at the Longest Wavelengths (DSL), in *2016 IEEE Aerospace Conference*, Big Sky, MT (2016), pp. 1–20. <https://doi.org/10.1109/AERO.2016.7500678>
- J.O. Bums, N. Duric, S. Johnson, G.J. Taylor, A lunar far-side very low frequency array. *NASA Conf. Publ.* **3039** (1989)
- J.O. Burns, J. Lazio, S. Bale, J. Bowman, R. Bradley, C. Carilli, S. Furlanetto, G. Harker, A. Loeb, J. Pritchard, Probing the first stars and black holes in the early universe with the Dark Ages Radio Explorer (DARE). *Adv. Space Res.* **49**, 433–450 (2012). <https://doi.org/10.1016/j.asr.2011.10.014>
- G.J. Feldman, R.D. Cousins, Unified approach to the classical statistical analysis of small signals. *Phys. Rev. D* **57**(7), 3873–3889 (1998). <https://doi.org/10.1103/PhysRevD.57.3873>
- Y. Futaana, S. Barabash, M. Wieser, M. Holmström, C. Lue, P. Wurz, A. Schaufelberger, A. Bhardwaj, M.B. Dhanya, K. Asamura, Empirical energy spectra of neutralized solar wind protons from the lunar regolith. *J. Geophys. Res.* **117**, E05005 (2012). <https://doi.org/10.1029/2011JE004019>
- J.W. Head, S. Murchie, J.F. Mustard, C.M. Pieters, G. Neukum, A. McEwen, R. Greeley, E. Nagel, M.J.S. Belton, Lunar impact basins: new data for the western limb and far side (Orientale and South Pole-Aitken Basins) from the first Galileo flyby. *J. Geophys. Res., Planets* **98**, 17149–17181 (1993). <https://doi.org/10.1029/93JE01278>
- X.Y. Hu, P. Ma, Y.Z. Yang, M.H. Zhu, T. Jiang, P.G. Lucey, L.Z. Sun, H. Zhang, C.L. Li, R. Xu, Z.P. He, H.Y. Lin, C.N. Huang, Y.X. Sun, Mineral abundances inferred from in situ reflectance measurements of Chang'E-4 landing site in South Pole-Aitken basin. *Geophys. Res. Lett.* **46**, 9439–9447 (2019). <https://doi.org/10.1029/2019GL084531>
- J. Huang, Z.Y. Xiao, J. Flahaut, M. Martinot, J.W. Head, X. Xiao, M.G. Xie, L. Xiao, Geological characteristic of Von Kármán crater, Northwestern South Pole Aitken basin: Chang'E 4 landing site region. *J. Geophys. Res.* **123**, 1684–1700 (2018). <https://doi.org/10.1029/2018JE005577>
- IAU WGPSN, Chang'e-4 Landing Site Name Approved: Statio Tianhe (Gazetteer of Planetary Nomenclature). <https://astrogeology.usgs.gov/news/nomenclature/chang-e-4-landing-site-name-approved-statio-tianhe>. Accessed 15 February 2019
- S. Jester, H. Falcke, Science with a lunar low-frequency array: from the dark ages of the Universe to nearby exoplanets. *New Astron. Rev.* **53**, 1–26 (2009). <https://doi.org/10.1016/j.newar.2009.02.001>
- A. Khan, J.A.D. Connolly, A. Pommier, J. Noir, Geophysical evidence for melt in the deep lunar interior and implications for lunar evolution. *J. Geophys. Res., Planets* **119**, 2197–2221 (2014). <https://doi.org/10.1002/2014JE004661>
- C.L. Li, J.J. Liu, X. Ren, W. Zuo, X. Tan, W.B. Wen, H. Li, L.L. Mu, Y. Su, H.B. Zhang, J. Yan, Z.Y. Ouyang, The Chang'e 3 mission overview. *Space Sci. Rev.* **190**, 85–101 (2015). <https://doi.org/10.1007/s11214-014-0134-7>
- C.L. Li, D.W. Liu, B. Liu, X. Ren, J.J. Liu, Z.P. He, W. Zuo, X.G. Zeng, R. Xu, X. Tan, X.X. Zhang, W.L. Chen, R. Shu, W.B. Wen, Y. Su, H.B. Zhang, Chang'E-4 initial spectroscopic identification of lunar far-side mantle-derived materials. *Nature* **569**, 378–382 (2019a). <https://doi.org/10.1038/s41586-019-1189-0>
- C.L. Li, C. Wang, Y. Wei, Y.T. Lin, China's present and future lunar exploration program. *Science* **365**, 238–239 (2019b). <https://doi.org/10.1126/science.aax9908>
- C.L. Li, Z.D. Wang, R. Xu, G. Lv, L.Y. Yuan, Z.P. He, J.Y. Wang, The scientific information model of Chang'e-4 Visible and Near-IR Imaging Spectrometer (VNIS) and in-flight verification. *Sensors* **19**(12), 2806 (2019). <https://doi.org/10.3390/s19122806>

- C.L. Li, Y. Su, E. Pettinelli, S.G. Xing, C.Y. Ding, J.J. Liu, X. Ren, S.E. Lauro, F. Soldovieri, X.G. Zeng, X.Y. Gao, W.L. Chen, S. Dai, D.W. Liu, G.L. Zhang, W. Zuo, W.B. Wen, Z.B. Zhang, X.X. Zhang, H.B. Zhang, The Moon's farside shallow subsurface structure unveiled by Chang'E-4 Lunar Penetrating Radar. *Sci. Adv.* **6**, 1–8 (2020). <https://doi.org/10.1126/sciadv.aay6898>
- H.L. Lin, Z.P. He, W. Yang, Y.T. Lin, R. Xu, C. Zhang, M.H. Zhu, R. Chang, J.H. Zhang, C.L. Li, H.Y. Lin, Y. Liu, S. Gou, Y. Wei, S. Hu, C.B. Xue, J.F. Yang, J. Zhong, X.H. Fu, W.X. Wan, Y.L. Zou, Olivine-norite rock detected by the lunar rover Yutu-2 likely crystallized from the SPA impact melt pool. *Nat. Sci. Rev.* **7**(5), 913–920 (2019). <https://doi.org/10.1093/nsr/nwz183>
- Z.C. Ling, L. Qiao, C.Q. Liu, H.J. Cao, X.Y. Bi, X.J. Lu, J. Zhang, X.H. Fu, B. Li, J.Z. Liu, Composition, mineralogy and chronology of mare basalts and non-mare materials in Von Kármán crater: landing site of the Chang'E-4 mission. *Planet. Space Sci.* **179**, 104741 (2019). <https://doi.org/10.1016/j.pss.2019.104741>
- J.J. Liu, X. Ren, W. Yan, C.L. Li, H. Zhang, Y. Jia, X.G. Zeng, W.L. Chen, X.G. Zeng, X.Y. Gao, D.W. Liu, X. Tan, X.X. Zhang, T. Ni, H.B. Zhang, W. Zuo, Y. Su, W.B. Wen, Descent trajectory reconstruction and landing site positioning of Chang'E-4 on the lunar farside. *Nat. Commun.* **10**(4229), 1–10 (2019). <https://doi.org/10.1038/s41467-019-12278-3>
- J.E. Mazur, W.R. Crain, M.D. Looper, D.J. Mabry, J.B. Blake, A.W. Case, M.J. Golightly, J.C. Kasper, H.E. Spence, New measurements of total ionizing dose in the lunar environment. *Space Weather* **9**, S07002 (2011). <https://doi.org/10.1029/2010SW000641>
- D.J. McComas, F. Allegrini, P. Bochsler, P. Frisch, H.O. Funsten, M. Gruntman, P.H. Janzen, H. Kucharek, E. Möbius, D.B. Reisenfeld, N.A. Schwadron, Lunar backscatter and neutralization of the solar wind: first observations of neutral atoms from the moon. *Geophys. Res. Lett.* **36**, L12104 (2009). <https://doi.org/10.1029/2009GL038794>
- K. Miljković, M.A. Wiczeorek, G.S. Collins, M. Laneuville, G.A. Neumann, H.J. Melosh, S.C. Solomon, R.J. Phillips, D.E. Smith, M.T. Zuber, Asymmetric distribution of lunar impact basins caused by variations in target properties. *Science* **342**, 724–726 (2013). <https://doi.org/10.1126/science.1243224>
- K. Pahlevan, D.J. Stevenson, Equilibration in the aftermath of the lunar forming giant impact. *Earth Planet. Sci. Lett.* **262**, 438–449 (2007). <https://doi.org/10.1016/j.epsl.2007.07.055>
- N.E. Petro, C.M. Pieters, Surviving the heavy bombardment: ancient material at the surface of South Pole-Aitken basin. *J. Geophys. Res.* **109**, E06004 (2004). <https://doi.org/10.1029/2003JE002182>
- C.M. Pieters, S. Tompkins I, J.W. Head, P.C. Hes, Mineralogy of the mafic anomaly in the South Pole-Aitken basin: implications for excavation of the lunar mantle. *Geophys. Res. Lett.* **24**, 1903–1906 (1997). <https://doi.org/10.1029/97GL01718>
- G. Reitz, T. Berger, D. Matthiae, Radiation exposure in the moon environment. *Planet. Space Sci.* **74**, 78–83 (2012). <https://doi.org/10.1016/j.pss.2012.07.014>
- A.E. Ringwood, *Origin of the Earth and Moon* (Springer, New York, 1979), pp. 198–228
- D.J. Stevenson, Lunar asymmetry and palaeomagnetism. *Nature* **287**, 520–521 (1980). <https://doi.org/10.1038/287520a0>
- Z.Z. Sun, H. Zhang, X.Y. Wu, F. Li, M. Yang, M. Cheng, Y.Q. Xu, Y.W. Zhang, Flight results of Chang'E-4 lander summary and evaluation. *Sci. Sin. Technol.* **49**, 1397–1407 (2019). <https://doi.org/10.1360/SST-2019-0106>. (In Chinese)
- Y.D. Takahashi, A concept for a simple radio observatory at the lunar South pole. *Adv. Space Res.* **31**, 2473–2478 (2003). [https://doi.org/10.1016/S0273-1177\(03\)00540-4](https://doi.org/10.1016/S0273-1177(03)00540-4)
- W.M. Vaughan, J.W. Head, Impact melt differentiation in the South Pole-Aitken basin: some observations and speculations. *Planet. Space Sci.* **91**, 101–106 (2014). <https://doi.org/10.1016/j.pss.2013.11.010>
- P.H. Warren, The magma ocean concept and lunar evolution. *Annu. Rev. Earth Planet. Sci.* **13**, 201–240 (1985). <https://www.annualreviews.org/doi/pdf/10.1146/annurev.ea.13.050185.001221>
- M. Wieser, S. Barabash, Y. Futaana, M. Holmström, A. Bhardwaj, R. Sridharan, M.B. Dhanya, A. Schaufelberger, P. Wurz, First observation of a mini-magnetosphere above a lunar magnetic anomaly using energetic neutral atoms. *Geophys. Res. Lett.* **37**, L05103 (2010). <https://doi.org/10.1029/2009GL041721>
- M. Wieser, S. Barabash, X.D. Wang, C. Lue, A.B. Zhang, C. Wang, W.J. Wang, Solar wind interaction with the lunar surface: observations by the advanced small analyzer for neutrals on the rover of Chang'E-4, in *EGU General Assembly 2019* vol. 13 (2019). EPSC-DPS2019-808-1
- M. Wieser, S. Barabash, X.D. Wang, A.B. Zhang, C. Wang, W.J. Wang, Solar wind interaction with the lunar surface: observation of energetic neutral atoms on the lunar surface by the Advanced Small Analyzer for Neutrals (ASAN) instrument on the Yutu-2 rover of Chang'E-4. *EGU General Assembly* (2020). <https://doi.org/10.5194/egusphere-egu2020-9199>
- D.E. Wilhelms, J.F. McCauley, N.J. Trask, The geologic history of the Moon. Technical Report. USGS professional paper 1348, 245 (1987)
- R.F. Wimmer-Schweingruber, S.Y. Zhang, J. Yu, S.I. Böttcher, S. Burmeister, H. Lohf, B. Yuan, G.H. Shen, C. Wang, J.N. Guo, Z.G. Xu, T. Berger, C. Hellweg, D. Matthiae, First results from the Lunar Lander Neutron and Dosimetry experiment (LND) on China's Chang'E 4 mission to the far side of the Moon, in *2019 EPSC-DPS Joint Meeting*, vol. 13 (2019). EPSC-DPS2019-1289-1

- R.F. Wimmer-Schweingruber, J. Yu, S.I. Böttcher, S.Y. Zhang, S. Burmeister, H. Lohf, J.N. Guo, Z.G. Xu, B. Schuster, L. Seimetz, J.F.V. Forstner, A. Ravanbakhsh, V. Knierim, S. Kolbe, H. Woyciechowski, S.R. Kulkarni, B. Yuan, G.H. Shen, C.Q. Wang, Z. Chang, T. Berger, C.E. Hellweg, D. Matthä, D.H. Hou, A. Knappmann, C. Büschel, X.F. Hou, B.G. Ren, Q. Fu, The Lunar Lander Neutron and Dosimetry (LND) experiment on Chang'E 4. *Space Sci. Rev.* **216**, 104 (2020). <https://doi.org/10.1007/s11214-020-00725-3>
- J.A. Wood, Bombardment as a cause of the lunar asymmetry. *Moon* **8**, 73–103 (1973). <https://doi.org/10.1007/BF00562751>
- W.R. Wu, Q. Wang, Y.H. Tang, G.B. Yu, J.Z. Liu, W. Zhang, Y.M. Ning, L.L. Lu, Design of Chang'E-4 lunar farside soft-landing mission. *J. Deep Space Explor.* **4**(2), 111–117 (2017). <https://doi.org/10.15982/j.issn.2095-7777.2017.02.002>. (In Chinese)
- W.R. Wu, C.L. Li, W. Zuo, H.B. Zhang, J.J. Liu, W.B. Wen, Y. Su, X. Ren, J. Yan, D.Y. Yu, G.L. Dong, C. Wang, Z.Z. Sun, E.H. Liu, J.F. Yang, Z.Y. Ouyang, Lunar farside to be explored by Chang'e-4. *Nat. Geosci.* **12**, 222–223 (2019). <https://doi.org/10.1038/s41561-019-0341-7>
- P. Wurz, S.A. Fuselier, E. Möbius, H.O. Funsten, P.C. Brandt, F. Allegrini, A.G. Ghielmetti, R. Harper, E. Hertzberg, P. Janzen, H. Kucharek, D.J. McComas, E.C. Roelof, L. Saul, J. Scheer, M. Wieser, Y. Zheng, IBEX backgrounds and signal-to-noise ratio. *Space Sci. Rev.* **146**, 173 (2009). <https://doi.org/10.1007/s11214-009-9515-8>
- L. Xiao, China's touch on the Moon. *Nat. Geosci.* **7**, 391–392 (2014). <https://doi.org/10.1038/ngeo2175>
- P.J. Ye, Z.Z. Sun, H. Zhang, F. Li, An overview of the mission and technical characteristics of Change'4 Lunar Probe. *Sci. China, Technol. Sci.* **60**, 658–667 (2017). <https://doi.org/10.1007/s11431-016-9034-6>
- P.J. Ye, Z.Z. Sun, H. Zhang, L.H. Zhang, X.Y. Wu, F. Li, Mission design of Chang'e-4 probe system. *Sci. Sin. Technol.* **49**, 124–137 (2019). <https://doi.org/10.1360/N092018-00400>. (In Chinese)
- S.Y. Zhang, R.F. Wimmer-Schweingruber, J. Yu, C. Wang, Q. Fu, Y.L. Zou, Y.Q. Sun, C.Q. Wang, D.H. Hou, S.I. Böttcher, S. Burmeister, L. Seimetz, B. Schuster, V. Knierim, G.H. Shen, B. Yuan, H. Lohf, J.N. Guo, Z.G. Xu, J.L. Freiherr von Forstner, S.R. Kulkarni, H.T. Xu, C.B. Xue, J. Li, Z. Zhang, H. Zhang, T. Berger, D. Matthä, C.E. Hellweg, X.F. Hou, J.B. Cao, Z. Chan, B.Q. Zhang, Y.S. Chen, H. Geng, Z.D. Quan, First measurements of the radiation dose on the lunar surface. *Sci. Adv.* **6**, eaaz1334 (2020a). <https://doi.org/10.1126/sciadv.aaz1334>
- A.B. Zhang, M. Wieser, C. Wang, S. Barabash, W.J. Wang, X.D. Wang, Y.L. Zou, L. Li, J.B. Cao, L. Kalla, L. Dai, J. Svensson, L.G. Kong, M. Oja, B. Liu, V. Alatalo, Y.T. Zhang, J. Talonen, Y.Q. Sun, M. Emanuelsson, C.B. Xue, L. Wang, F. Wang, W.L. Liu, Emission of energetic neutral atoms measured on the lunar surface by Chang'E-4. *Planet. Space Sci.* **189**, 104970 (2020b). <https://doi.org/10.1016/j.pss.2020.104970>